Master Thesis

Polarimetric Calibration of a Bistatic SAR detector

Author: Luis Eduardo Yam Ontiveros
Directors: Dr. Jordi J. Mallorqui / Dr. Xavier Fábregas

Universitat Politècnica de Catalunya (UPC)
Department of Signal Theory and Communications (TSC)

July 2010

Contents

Introduction **1**

1 Radar framework **3**

1.1 Polarization of the electromagnetic waves 3

1.2 Scattering 6

1.2.1 Radar cross section 6

1.2.2 The scattering Matrix 7

1.3 Basis of Synthetic aperture radar 8

1.3.1 Resolution in the cross-track direction 9

1.3.2 Resolution in the azimuth direction 12

1.3.3 Synthetic Aperture Radar 12

1.4 Bistatic radars and SABRINA system 14

1.4.1 Ground range and azimuth resolution 14

2 Model of the system and calibration basis **17**

2.1 Description of polarimetric measurements in SAR systems 17

2.2 Coordinate system 18

2.3 System configuration 18

2.3.1 Sources of error 20

2.4 Calibration of the system 21

2.5 Retrieving the S-matrix of a target 23

2.6 Conclusions 23

3 PARCs: the calibration targets **24**

3.1 Scattering matrices of the PARCs 24

3.2 Alignment errors in One-PARC Configuration 27

3.2.1 Simulations 28
3.3 Alignment errors in Two-PARC Configuration 29
3.3.1 Simulations 33
3.4 Influence of the amplitude and phase response of the PARCs 34
3.4.1 One-PARC Configuration 36
3.4.2 Two-PARC Configuration 38
3.5 Conclusions 39

4 Experimental Campaing **41**
4.1 RADARSAT-2 41
4.2 PARC implementation 43
4.2.1 Structure 43
4.2.2 PARCs' antennas 43
4.2.3 Amplifiers 46
4.3 Outdoor experiments 50
4.3.1 Measurements and Results 51
4.3.2 Calibration 52
4.4 Conclusions 52
Conclusions 56

A Experimental Measurements **58**
A.1 Frequency response of amplifiers 2 and 3 58

List of Figures

1.1 Electromagnetic wave with: a) elliptical polarization, b) lineal polarization, and c) circular polarization 4
1.2 Decomposition of the electrical field in its horizontal and vertical components . 4
1.3 Elliptical polarization and geometrical relation of the parameters a_h, a_v, E_h, E_v, τ,and ϵ 6
1.4 Radar remote sensing systems: a) bistatic and b)monostatic configurations . . 9
1.5 Basic radar imaging geometry 10
1.6 Geometry of the resolution of the system 11
1.7 Chirp signal. a) Example of a chirp pulse, b) compressed chirp pulse 11
1.8 Diagram of the SAR system. The platform motion is used to synthesise a longer antenna. 13
1.9 SABRINA system. a) Bistatic geometry, b) Diagram of the dual channel receiver. 15

2.1 Pulse Switching required for measuring the Scattering parameters of a target . 18
2.2 Local coordinate systems in Back Scatter alignment (BSA) 19
2.3 Model of measurements in the bistatic sensor of oportunity 20

3.1 (a) Basic diagram of the PARCs, (b) general case for the antenna positioning of the PARCs 26
3.2 Relative error (%) of the estimated values of [C] as a function of θ and ϕ for the One-PARC configuration. a) $\tilde{c}_{11}$, b) $\tilde{c}_{22}$, c) $\tilde{c}_{33}$, d) $\tilde{c}_{44}$. SNR = 60 dB 30
3.3 Relative errors of the coefficients $\tilde{c}_{ii}$ for $\phi = -7^\circ$ and θ between $\pm 10^\circ$. SNR = 60dB 31
3.4 Relative errors (%) of coefficients from the scattering matrix of PARC-2. (a)$\tilde{s}_{hh}$ and (b)$\tilde{s}_{hh}$ as functions of θ and ϕ. SNR = 60dB 32

3.5 Relative error (%) of the estimated values of [**C**] as a function of θ and ϕ for the case of Two-PARC configuration. a) $\tilde{c}_{11}$, b) $\tilde{c}_{33}$. SNR = 60 dB 33
3.6 Relative error (%) of $\tilde{c}_{11}$ in Two-PARC configuration, a) function of $\theta(\phi = 0\,^\circ)$, b) function of $phi(\theta = 0\,^\circ)$. SNR =60 dB. 34
3.7 Relative errors (%) in (a)$\tilde{s}_{hh}$ and (b)$\tilde{s}_{vh}$ of the scattering matrix of PARC-1 as function of θ and ϕ. SNR = 60dB. 35
3.8 Magnitude of two S-parameters retrieved from PARC-2 (target) as a function of A_1; a)$\tilde{s}_{hh}$, b)$\tilde{s}_{hv}$. SNR =60dB 37
3.9 Phase of two S-parameters retrieved from PARC-2 (target) as a function of γ_1; a)$\tilde{s}_{hh}$, b)$\tilde{s}_{hv}$. SNR =60dB 37
3.10 Estimation of of PARC-1's s_{hh} (target), a) magnitud as a function of A_2, b)phase as a function of γ_2. SNR =60dB 39

4.1 a) Interleaved H and V pulses from RADARSAT-2 transmitted signal. Pulses with larger amplitude correspond to the V polarization. b) SABRINA system . 42
4.2 PARC configuration for calibration: a) One-PARC configuration, b) Two-PARC configuration. 44
4.3 Prototype of the structure for the PARCs. 45
4.4 Physical dimensions of the linear polarized horn antenna. 45
4.5 Radiation pattern of the horn antenna: a) Plane E, b) Plane H, c)3-D. Beamwidth $\sim 20\,^\circ$ 47
4.6 $|S_{11}|$, $|S_{22}|$, and $|S_{21}|$ of the three amplifiers used in the PARCs. a) Amplifier-1, b) Amplifier-2, and c) Amplifier-3. 48
4.7 S_{21} of Amplifier-1 at different external temperatures, a) magnitude, b)phase. . 49
4.8 Amplifier 1. a)Magnitude and b)phase of S_{21} as a function of the temperature at 5.4 GHz. 49
4.9 Location of the three PARCs and SAR detector. Red dot denotes the ONE-PARC configuration, and Blue dots denote the Two-PARC configuration. The shadowed area represents the $20\,^\circ$ beamwidth of the SAR sensor's antenna. . . 51
4.10 Direct measurements in dB: a)HH , b)HV, c)VH, d)VV 53
4.11 Calibrated measurements in dB with the Two-PARC configuration: a)HH , b)HV, c)VH, d)VV 54

A.1 S_{21} of Amplifier-2 at different external temperatures, a) magnitude, b)phase. . 58

A.2 S_{21} of Amplifier-2 at different external temperatures, a) magnitude, b)phase. . 59
A.3 Amplifier 2. a)Magnitude and b)phase of S_{21} as a function of the temperature at 5.4 GHz. 59
A.4 Amplifier 3. a)Magnitude and b)phase of S_{21} as a function of the temperature at 5.4 GHz. 60

Abstract

The polarimetric radars offer the advantage of knowing about properties of target's surface by acquiring information of how the incident electromagnetic energy is scattered respect to orthogonal polarization vectors. Bistatic sensors of opportunity, such as SABRINA, can be adapted to perform polarimetric measurements if they found an illuminator which transmits pulses with orthogonal polarizations. In such scenario, calibration is required to scale properly the measurements in magnitude and phase in order to be able to interpret the data. In this work, we use the concepts of calibration in the monostatic case to obtain and study a polarimetric calibration based on PARCs for a bistatic sensor of opportunity.

Introduction

Microwave Remote sensing and imaging has become an important tool for the study and undertanding of natural phenomena of our environment. We can find technologies that have evolved during the past 50 years, reaching maturity in active and passive applications. Researches and scientist have taken great advantages of the technology developed aimed to the measurement of different geographic parameters at global scale, or the imaging at different wavelengths to complement optical observations [1].

Other radar applications are still in the process to mature and offer a wide horizon of possibilities. This is the case of the bistatic radar. One of the attractive lines-of-work has been the implementation of systems that use signal of opportunity from existing radar transmitters. Moreover, this bistatic radar system can be implemented in a polarimetric configuration of the signal of opportunity offers polarization diversity.

The polarimetric radars offer a great advantage over classical single polarization radar since much more information can be recollected regarding the properties of target's surface. Knowledge about how the incident electromagnetic energy is scattered by a target can be inferred through polarimetry. However, the cost to pay is the calibration in order to be able to interpret correctly the data from measurement. In polarimatric applications, there are combinations of data from different channels to provide information about the nature of the target, and the proper scale in magnitude and phase of the measurement is required at the end of the transmitter-target-receiver chain[2].

For the calibration of polarimetric radars in monostatic configuration, there are several well-known techniques that have been effectively proven in field conditions[3]. Many of these techniques use passive elements such as reflector corners, disks or dipoles, but there are other examples in which the use active devices are proposed for the calibration.

In this sense, transponders or PARCs (*Polarimetric Active Radar Calibrator*) offers the advantage of wide beamwidths, compactness and high signal-to-background clutter ratio[3]. On the other hand, in bistatic configuration, calibration techniques have been mainly studied in laboratory conditions due to the sensitivity of the calibration towards the alignment errors of control targets[4, 5].

The Remote Sensing Laboratory at UPC has successfully implemented a bistatic radar systems, the so-called SABRINA[6]. The maturity of SABRINA system has allowed the adaptation of performing polarimetric measurements by using signals of opportunity containing pulses in two orthogonal polarizations such as RADARSAT-2's signal. For the proper analysis of the data, a calibration technique has to be implemented in field conditions due to the nature of the measurements. In this work, we apply concepts of the calibration in the monostatic case to the bistatic configuration in order to obtain a polarimetric calibration based on PARCs for the SAR detector. Moreover, this coarse approach is also focus on identify future lines of work for the improvement of the calibration procedure.

This work is divided in five chapters. The first Chapter is devoted to an introduction to radar terms and an overview of the *synthetic aperture radar* (SAR) technique. In the second chapter, we describe the conceptual model of the bistatic radar system, the sources of error which may distort the measurements, and the polarimetric calibration procedure. In the third chapter, we discuss the errors due the misalignment of the PARCs' antennas and assumptions about their scattering parameters. The fourth chapter describes the experimental implementation of the PARCs and qualitative results on the experimental campaign of July 7th, 2010. Finally, we finish with the conclusions and futures lines in the sixth fifth chapter.

Chapter 1

Radar framework

The Radar (*RAdio Detection And Ranging*) is an active microwave sensor that has been evolving over last 50 years. It is defined as a device for transmitting electromagnetic (EM) signals and receiving echoes from objects of interest (targets) within its volume of coverage [7]. In this sense, *a priori* knowledge of properties of the transmitted signals is the key to relate the echoes with physical properties of a target. Consequently, through the proper signal processing of the echoes(scattered signals), we can obtain information about present of the target, location, velocity or,in some cases, type of target.

1.1 Polarization of the electromagnetic waves

The polarization of a radiated electromagnetic wave is the property that describes the figure traced as a function of time by the extremity of the electric field vector at a fixed location in space, and the sense in which it is traced, as observed along the direction of propagation [8]. In general, the figure that the electric field traces is an ellipse. In that case, it is said that the field is *elliptically polarized*. However, we usually find in the radar systems special cases of the elliptical polarization: lineal and circular. Figure 1.1 shows the traces for electromagnetic waves with elliptical, lineal and circular polarization.

For remote sensing applications where the transmitting antenna is placed on an airplane or satellite, the electric field vector can be represented (locally) in terms of vertical and horizontal components with respect to the plane of incidence and the surface (figure 1.2). For the general case, we have the field vector [1]:

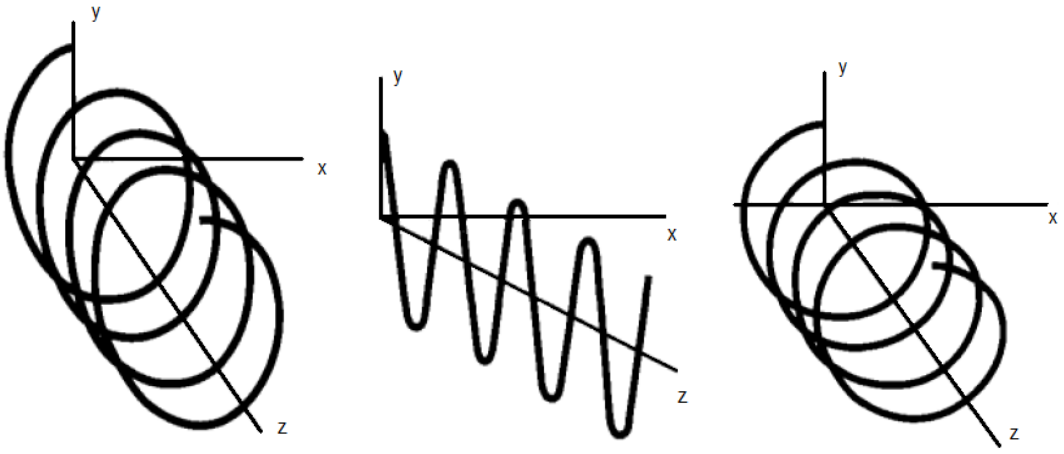

(a) (b) (c)

Figure 1.1: Electromagnetic wave with: a) elliptical polarization, b) lineal polarization, and c) circular polarization

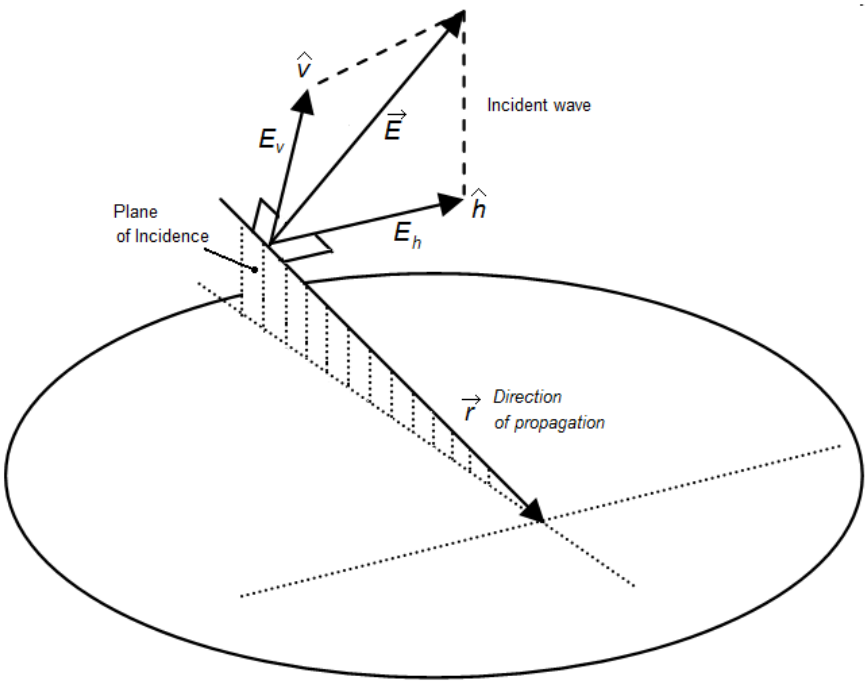

Figure 1.2: Decomposition of the electrical field in its horizontal and vertical components

$$\vec{E} = E_h\hat{h} + E_v\hat{v} = a_h\cos(\omega t - kr)\,\hat{h} + a_v\cos(\omega t - kr + \delta)\,\hat{v} \tag{1.1}$$

where $a_{h,v}$ is the amplitude of the corresponding components, r the direction of propagation,k the wavenumber, ω the angular frequency of the wave, and δ is a phase difference between a_h and a_v. The components E_h and E_v can be combined to give:

$$\left(\frac{E_h}{a_h}\right)^2 + \left(\frac{E_v}{a_v}\right)^2 - 2\frac{E_hE_v}{a_ha_v}\cos\delta = \sin\delta^2 \tag{1.2}$$

Equation 1.2 represents an ellipse centered in the origin(figure1.3). From there, we can differentiate the three polarization states with the difference values of the parameters a_h, a_v and δ:

- The *linear polarization* is achieved when

$$\delta = n\pi, \quad n = 0, 1, 2, 3, \ldots$$

- The *circular polarization* is achieved only when $a_v = a_h$, and

$$\delta = \begin{cases} +\left(\frac{1}{2} + 2n\right)\pi, n = 0, 1, 2, \ldots & \text{RH polarization} \\ -\left(\frac{1}{2} + 2n\right)\pi, n = 0, 1, 2, \ldots & \text{LH polarization} \end{cases}$$

- The *elliptical polarization* is achieved only when

$$a_v \neq a_h \text{ and } \delta = \begin{cases} +\left(\frac{1}{2} + 2n\right)\pi, n = 0, 1, 2, \ldots & \text{RH polarization} \\ -\left(\frac{1}{2} + 2n\right)\pi, n = 0, 1, 2, \ldots & \text{LH polarization} \end{cases}$$

$$\text{or } \delta \neq \begin{cases} +\frac{n}{2}\pi, n = 0, 1, 2, \ldots & \text{RH polarization} \\ -\frac{1}{2}\pi, n = 0, 1, 2, \ldots & \text{LH polarization} \end{cases}$$

where *RH* adn *LH* refers to *right-hand* and *left-hand* polarization. The parameters a_h, a_v, and δ can be fully described by two properties of the ellipse in figure 1.3. The first one is the *ellipticity*, ϵ, which describes how close is the ellipse from a circle. The second one is the *tilt*, τ, with respect to the horizontal. From the elliptical figure, the relationships between the properties (a_h, a_v, δ) and (τ, ϵ) [1] are

$$\tan 2\tau = \tan\left(2\tan^{-1}\frac{a_v}{a_h}\right)\cos\delta \tag{1.3}$$

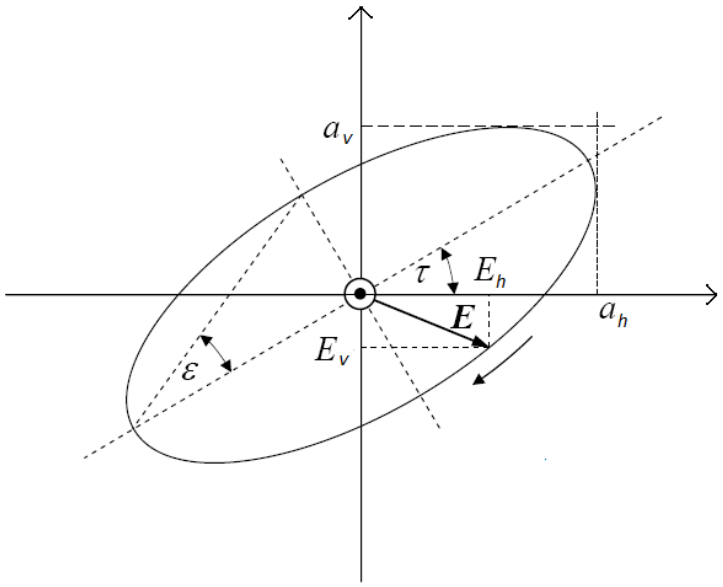

Figure 1.3: Elliptical polarization and geometrical relation of the parameters a_h, a_v, E_h, E_v, τ,and ϵ

$$\sin 2\epsilon = \sin\left(2\tan^{-1}\frac{a_v}{a_h}\right)\sin\delta \tag{1.4}$$

Notice that for the ellipticity, the range of values is $-\pi/4 \leq \epsilon \leq \pi/4$, and for the tilt we have that $-\pi/2 \leq \tau \leq \pi/2$

1.2 Scattering

1.2.1 Radar cross section

The radar can be used as a remote sensing device due to the interaction of the electromagnetic waves with objects. A fundamental equation that relates the power (P_t) of the transmitted wave with the power received (P_r) by the radar system is the *radar equation*(equation 1.5). This equation describes the maximum range of a radar when all terms are known as well as the limit of power detection at the receiver.

$$P_r = \frac{P_t G_t G_r \lambda^2 \sigma}{(4\pi)^3 R^4} \tag{1.5}$$

where G_t is the gain of the transmitting antenna, G_r the gain of the receiving antenna, λ the work frequency of the radar, R the distance from the radar to the target, and σ the *radar cross section.*

In general, any targets present a cross section area for the incoming radiation. The *Radar Cross Section* describes how much of that incident energy reflected(scattered) by the target. Theoretically, the *RCS (σ)* is defined as the cross section of an equivalent idealized isotropic scatterer that generates the same scattered power density as the target in the observed direction:

$$\sigma = \lim_{R\to\infty} 4\pi R^2 \frac{|E^r|^2}{|E^i|^2} \tag{1.6}$$

where R is the radio of the sphere centered in the target position. The limit on R implies the far field condition. In general, scattering properties of the target are likely to change for different polarization of the incident wave. Moreover, the scattered waves may have a different polarization than the incident one. All that phenomena is used in radar remote sensing applications to identify targets on the Earth's surface[1]. In order to denote such polarization dependence in the scattering properties of the target, the *RCS* can be represented in a matricial form. For instance, for the case of H and V orthogonal polarization we would have:

$$RCS = \begin{bmatrix} \sigma_{hh} & \sigma_{hv} \\ \sigma_{vh} & \sigma_{vv} \end{bmatrix} \tag{1.7}$$

where σ_{hv} indicate that the incident wave has H polarization, and the scattered wave has V polarization.

1.2.2 The scattering Matrix

The *scattering matrix* describes the polarimetric behavior a of scatterer through the relationship between the incident and scattered electric fields. Thus, it is possible to decompose the scattered field in terms of the transverse components of the electric field of the incident wave. Assuming vertical and horizontal components of the fields, we have

$$\begin{bmatrix} E_h^s \\ E_v^s \end{bmatrix} = \begin{bmatrix} S_{hh} & S_{hv} \\ S_{vh} & S_{vv} \end{bmatrix} \begin{bmatrix} E_h^i \\ E_v^i \end{bmatrix} \tag{1.8}$$

with $[E]^s$ the scattered electric field, $[E]^i$ the incident electric field, and $[S]$ the scattering matrix. The previous expression can be modified considering that the scattering properties are observed in the far field at a distance R by the radar, then:

$$\begin{bmatrix} E_h^r \\ E_v^r \end{bmatrix} = \frac{e^{jkR}}{R} \begin{bmatrix} S_{hh} & S_{hv} \\ S_{vh} & S_{vv} \end{bmatrix} \begin{bmatrix} E_h^i \\ E_v^i \end{bmatrix} \tag{1.9}$$

The elements in the scattering coefficients are related with the RCS σ_{PQ}. From the definition of the RCS in equation 1.6:

$$\sigma_{PQ} = 4\pi R^2 \frac{|E_P^r|^2}{\left|E_Q^i\right|^2}$$

since $|E_P^r| = \frac{e^{jkR}}{R}\left|E_Q^s\right|$, and omitting the phase propagation that is not relevant for the power quantities [1], the RCS is

$$\sigma_{PQ} = 4\pi \frac{|E_P^s|^2}{\left|E_Q^i\right|^2}$$

And from 1.8

$$\sigma_{PQ} = 4\pi \left|S_{PQ}\right|^2 \tag{1.10}$$

1.3 Basis of Synthetic aperture radar

The radar is an *active* remote sensing device whose basic parts are a transmitter and a receiver of microwave energy. In remote sensing microwave imaging, we have two possible options for the location of the transmitter and receiver. In the *monostatic* case, they are placed at the same location (figure 1.4a), and sometimes using the same antenna for transmitting and receiving. This configuration has been the most commonly used in remote sensing systems [1]. The other option is the *bistatic* configuration in which transmitter and receiver are placed in different locations(figure 1.4b). The bistatic radar turns an interesting option since it can adopt the signal of illuminators of opportunity as their inputs[1].

In remote sensing applications, the radar is located in a moving platform such as a spacecraft or aircraft. Figure 1.5 depicts a typical monostatic radar configuration in stripmap mode. The antenna radiates the energy in a broad beam at a constant angle

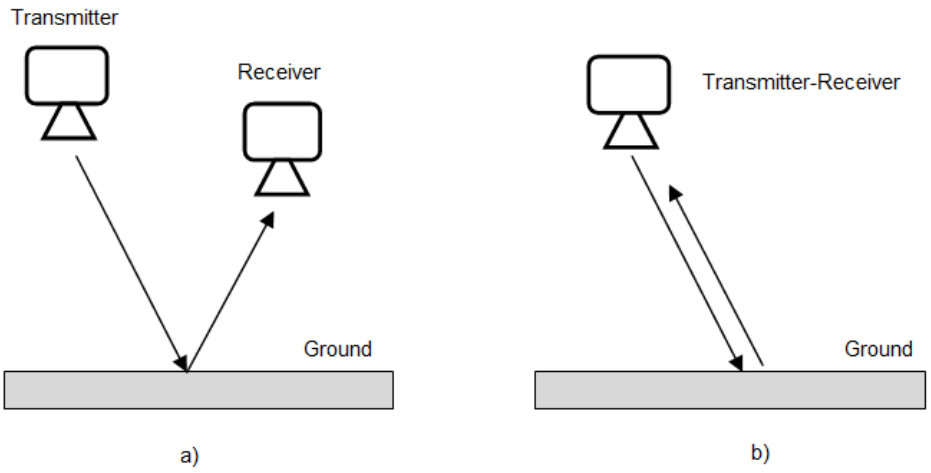

Figure 1.4: Radar remote sensing systems: a) bistatic and b)monostatic configurations

to the flight path, and its projection on the grown is actually defining the swath width. In the direction of the motion of the platform, usually the antenna beam is narrow.

1.3.1 Resolution in the cross-track direction

The resolution at the direction across the swath (*range direction*) is obtained through the classical principles of radar by transmitting pulses at the operating frequency of the radar and receiving back their echoes. The pulses are transmitted at a certain rate called *pulse repetition frequency (prf)*, which have the constrain on receiving most of the echoes in a time window between the pulses transmitted. Then, the largest *slang range* (distance from the satellite to a point on the ground) dictates an upper bound for the value of the *prf*. The duration of the pulse has influence on the cross-track resolution. If two targets on the ground are Δr apart (figure 1.6), we will have, roughly, a difference in time of the echoes of $\Delta t \approx \frac{2\Delta r}{c}$, being c the speed of light. The lower limit for Δt is the duration τ of the pulse. Thus, the slant range resolution r_r and ground range resolution are

$$\Delta r_r = \frac{c\tau}{2} \tag{1.11}$$

$$\Delta r_g = \frac{c\tau}{2\sin\theta} \tag{1.12}$$

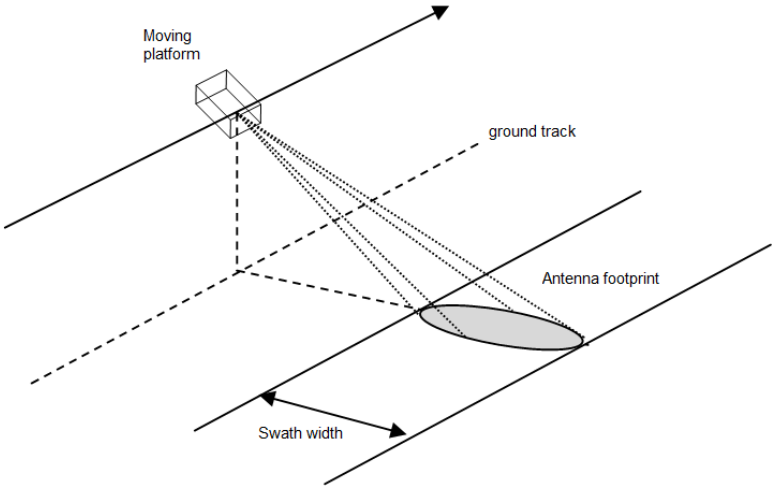

Figure 1.5: Basic radar imaging geometry

where θ represents the local angle of incidence of the radiation beam as shown in figure 1.6. Both slant and ground resolutions are independent of the altitude of the platform, but the latter is function of the local angle of incidence and vary across the swath. Moreover, better resolution is in the far swath, and better in the near swath.

In order to increase the spatial resolution, one can consider the option of reducing the duration of the pulses. However, if we consider a constant power, the energy of the pulses is reduced by narrowing them, limiting the sensitivity of the radar. A special signal, called *chirp*, is used to overcome that problem while increasing the resolution. The *chirp* signal is a pulse with large duration, which implies lower power peaks, and with wide bandwidth, which increase resolution. Within this pulse, the instant frequency is a linear function of the time as shown in figure 1.7(a). At the reception stage, the chirp is passed through a matched filter, resulting in a compressed pulse, which is the effective pulse for the range resolution(equation 1.7(b)). Equation 1.13 gives the mathematical expression of the chirp signal assuming a unity amplitud pulse $p(t)$, and equation 1.14 is related to expression of the compressed chirp.

$$c(t) = p(t)\cos\left(\omega_0 t + \pi\alpha t^2\right) \tag{1.13}$$

$$z(t) = \cos(\omega_0 t)\,\mathrm{sinc}(\pi BW_c t) \tag{1.14}$$

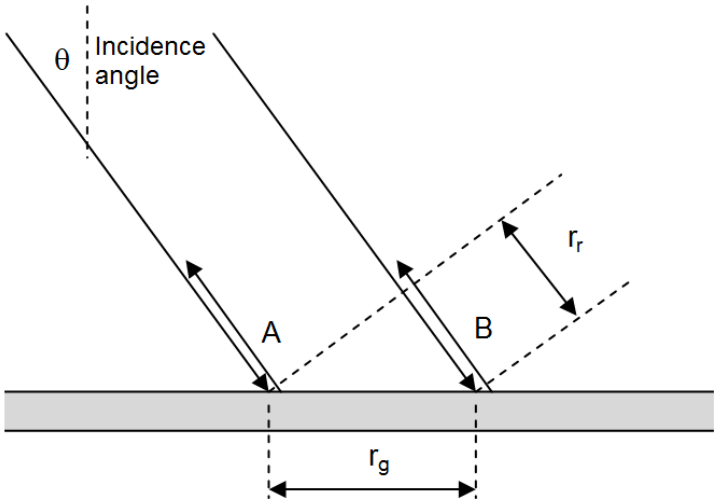

Figure 1.6: Geometry of the resolution of the system

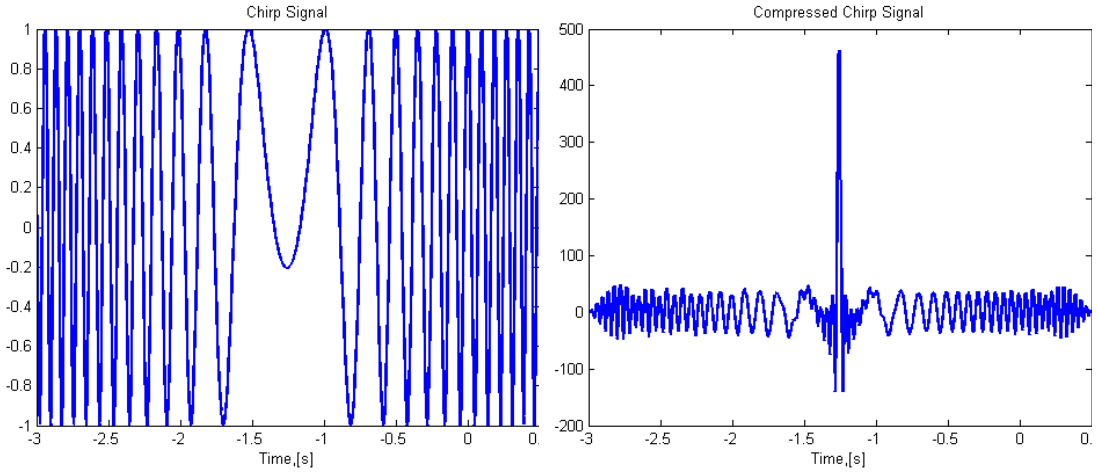

(a) (b)

Figure 1.7: Chirp signal. a) Example of a chirp pulse, b) compressed chirp pulse

where α is the *chirp rate*. From equation 1.14, the half power width is the reciprocal of the chirp bandwidth ($BW_c = \alpha\tau_r$)[1]. Then, with width of the compress pulse, the slant and ground resolution are improved:

$$\Delta r_r = \frac{c}{2BW_c} \tag{1.15}$$

$$\Delta r_g = \frac{c}{2BW_c \sin\theta} \tag{1.16}$$

1.3.2 Resolution in the azimuth direction

The azimuth resolution is given by the beamwidth of the antenna in the parallel direction along the motion of the platform. Assuming an antenna of length l_a in the azimuth direction, and that it is larger than the wavelength, we have that the angular beamwidth is approximately $\Theta_a = \frac{\lambda}{l_a}$, then the antenna footprint in that direction leads to a resolution of

$$\Delta r_a = \frac{\lambda}{l_a} R_0 \tag{1.17}$$

R_0 represents the distance from the platform to the ground. The azimuth resolution of that system depends on the altitude of the platform and the work frequency of the radar. The *synthetic aperture radar* technique can be used to enhance greatly the azimuth resolution and make it independent of the altitude and the wavelength.

1.3.3 Synthetic Aperture Radar

This method helps to increase the azimuth resolution by taking advantage of the lineal motion of the platform to synthesize a longer antenna. Figure 1.8 shows a diagram of the geometry in SAR. The registered echoes of a certain target on ground will have different delays. They will depend on how near or far is the target respect to the moving platform given by

$$t_D = \frac{2R(t)}{c} \approx \frac{2}{c}\left\{R_0 + \frac{(vt)^2}{2R_0}\right\} = \frac{4\pi R_0}{\lambda} + 2\pi\frac{v^2t^2}{\lambda R_0} = \frac{4\pi R_0}{\lambda} + \frac{1}{2}bt^2 \tag{1.18}$$

In most remote sensing radars, the radar bandwidth is much smaller than its carrier frequency, and we can make the approximation that the signal transmitted is a single

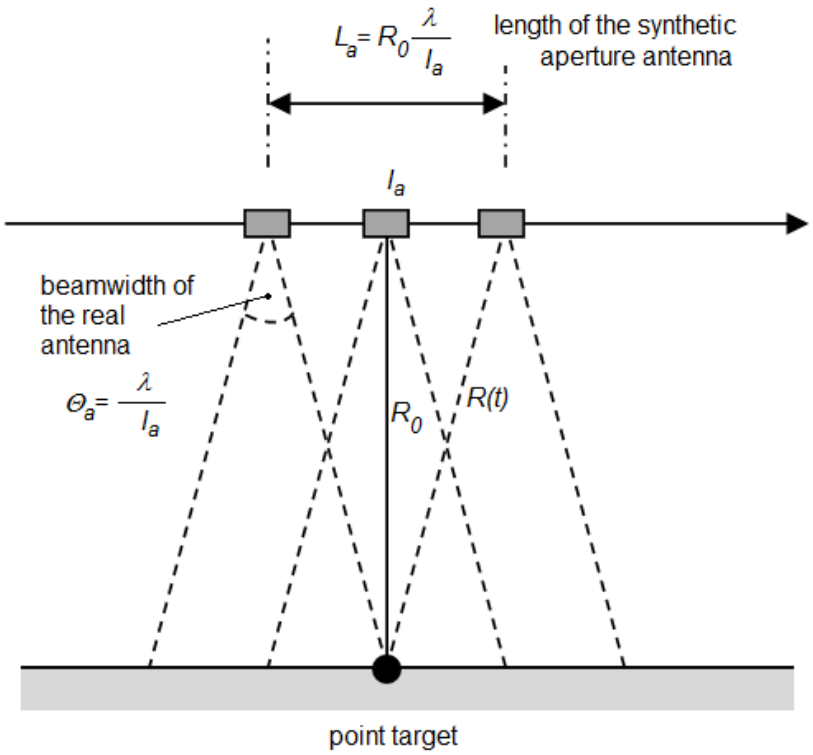

Figure 1.8: Diagram of the SAR system. The platform motion is used to synthesise a longer antenna.

sinusoidal $\cos \omega_c (t + t_D)$. The signal has a frequency variation because of the Doppler Effect. Moreover, the modified signal appears as a chirp, and it can be compressed as in the case of the range compression, but with an estimation of the Doppler induced chirp.

Similarly to the chirp signals in range, the time duration of the compressed chirp is $\tau_a = \frac{1}{BW_D}$. In this case $BW_D = bT_a = b\frac{L_a}{v}$, being $L_a = \frac{\lambda R_0}{l_a}$ the length of the synthetic aperture antenna(figure1.8). We can obtain the azimuth resolution by multiplying τ_a by the platform velocity:

$$\Delta r_a = \frac{v}{BW_D} = \frac{l_a}{2} \tag{1.19}$$

1.4 Bistatic radars and SABRINA system

In the bistatic case, the radar transmitter and receiver are placed in different locations. The configuration of interest for our framework is the one in which the transmitter is moving (e.g. a satellite) and the receiver is stationary on the Earth's surface. In fact, that is the configuration used by SABRINA (*SAR Bistatic Receiver for Interferometric Applications*)[6]. Figure 1.9(a) shows the geometry of such bistatic system.

SABRINA is a passive system since it uses the signals from satellites in C-band (such as ENVISAT or RADARSAT-2) as signals of opportunity for remote imaging. Since the receiver is not directly synchronized with the transmitter (i.e. the satellite), a replica of the transmitted signal is obtained through an antenna pointing directly to the satellite. In that manner, the synchronization is done directly with the transmitted signal [6]. A block diagram of SABRINA system is shown in figure 1.9(b).

1.4.1 Ground range and azimuth resolution

In the bistatic case, the transmitted signal and their echoes have different paths. Similar to the monostatic case, we have that the range resolution is $\Delta r = c \cdot \tau = \frac{c}{BWc}$. If we assume that the surface is locally flat, the ground resolution is close to

$$\Delta r_{g,bis} = \frac{c}{BW_c (\sin \theta_t + \sin \theta_r)} \tag{1.20}$$

Where BW_c is the bandwith of the chirp signal, θ_t is the incident angel of the transmitted signal and θ_r is the received angle of the scattered wave as shown in figure 1.9(a).

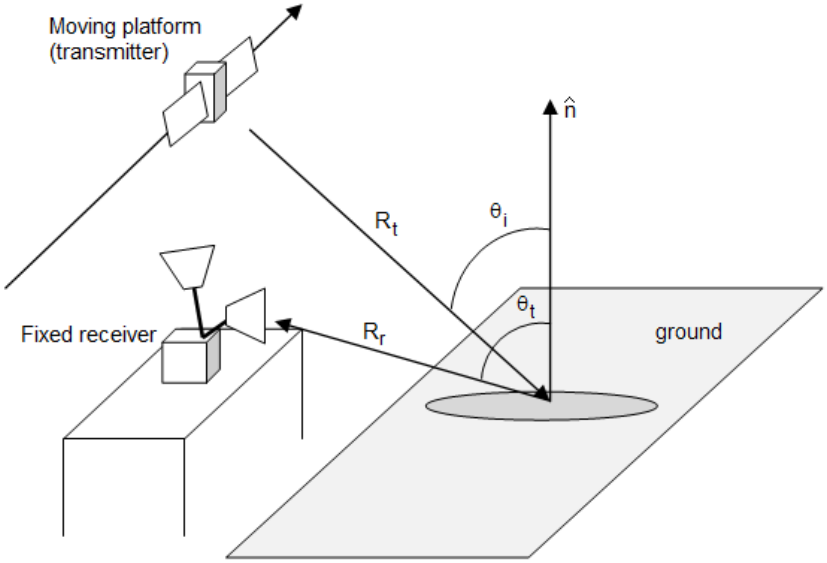

(a)

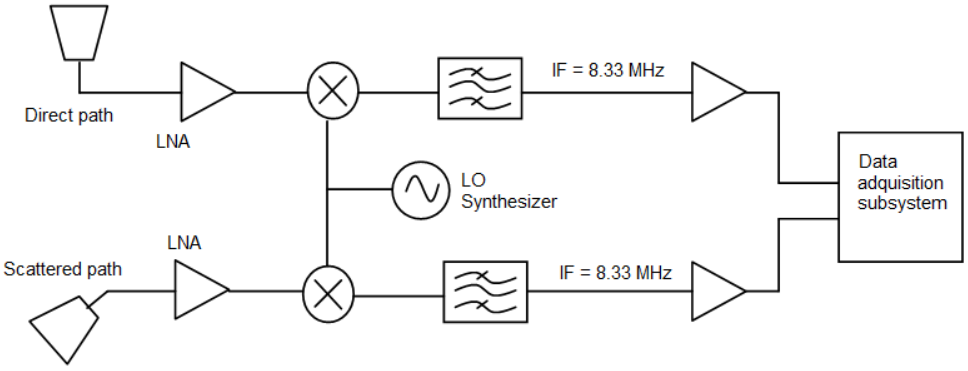

(b)

Figure 1.9: SABRINA system. a) Bistatic geometry, b) Diagram of the dual channel receiver.

Notice that the ground range resolution is improved with respect to the monostatic case if $\theta_r > \theta_i$.

Previously, it was described that the azimuth resolution for SAR systems is related to the velocity of the platform and the bandwidth of the chirp induced by the Doppler effect in the transmitted signal: $\Delta r = \frac{v}{BW_D}$. For the monostatic case it was assumed a two-way beamwidth $B_{2-way} \approx \frac{\lambda}{l_a}$, but in the bistatic case with a fixed receiver, only the one-way transmit beamwidth B_{1-way} is considered and the Doppler bandwidth $BW_D\prime$ results in $BW_D\prime = \frac{vB_{1-way}}{BW_D}$. If we approximate the beampattern by a Gaussian function, the ratio $\frac{B_{2-way}}{B_{1-way}}$ is $\sqrt{2}$ [6]. Thus, the bistatic azimuth resolution is:

$$\Delta r_{a,bist} = \frac{l_a}{\sqrt{2}} = \sqrt{2}\Delta r_{a,mono} \tag{1.21}$$

Chapter 2

Model of the system and calibration basis

2.1 Description of polarimetric measurements in SAR systems

The current SABRINA system [6] has been adapted to peform polarimetric measurements. PolSAR is an extension of SAR systems in which we can obtain measurements of the scattered electric field considering its polarization state. Thus, instead of having the measurement of a single complex number, we will have four complex numbers representing the scattering matrix of a target.

Polarimetric systems require the transmission of two orthogonal polarizations in order to estimate the four coefficients of the scattering matrix. Commonly, these polarizations are horizontal (H) and vertical (V) linear or left and right circular (L and R) [9].

The coefficients of the scattering matrix can be measure by pairs. When a signal of certain polarization is transmitted to the target, we measure in amplitude and phase, the scattered field components in the orthogonal polarization channels. For instance, considering H and V polarization, by having the signal transmitted in H, we measure the scattered fields in H and V in order to have the first column of the scattering matrix. Similarly, we obtain the measurements for the second column by measuring in both H and V channels, the scattered fields when the incidence signal is V polarized. Figure 2.1 illustrates the sequence of measurements to obtain the desired scattering matrix. In

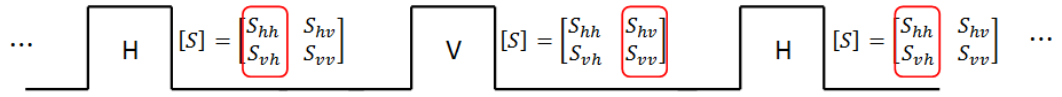

Figure 2.1: Pulse Switching required for measuring the Scattering parameters of a target

our case, the system is using signals of opportunity that come from the RADARSAT-2's emission, which interleaves H and V polarized pulses [10].

2.2 Coordinate system

In polarimetric radar application, the coordinate system must be established in order to avoid ambiguities in the description of the target. Usually, right-handed Cartesian coordinate systems are used locally at the transmitter for describing the polarization components of the electric field with respect to the direction of propagation. For the scattered fields, there are two conventions: *forward scatter alignment* (FSA) and *back scatter alignment* (BSA). The FSA is a right-handed Cartesian coordinate system which follows the propagation of the scattered waves. On the other hand, BSA is a right-handed Cartesian coordinate system that is placed locally at the receiver. The BSA convention is commonly use in backscattering applications, because the coordinate systems of the transmitting and receiving antenna coincide when they are located at same position. Figure 2.2 depicts the BSA convention and the relation of the local coordinate systems with respect to a global local system with origin within the scatterer. In that figure, the subscripts i and s indicate the incident and scattered field, respectively. For the follow, we will adopt this BSA convention.

2.3 System configuration

Polarimetric radar systems offer the advantage of acquiring richer information about the nature of different targets by processing the polarization of the scattered fields detected. However, this implies that the polarimetric measurements must be done, ideally, by a

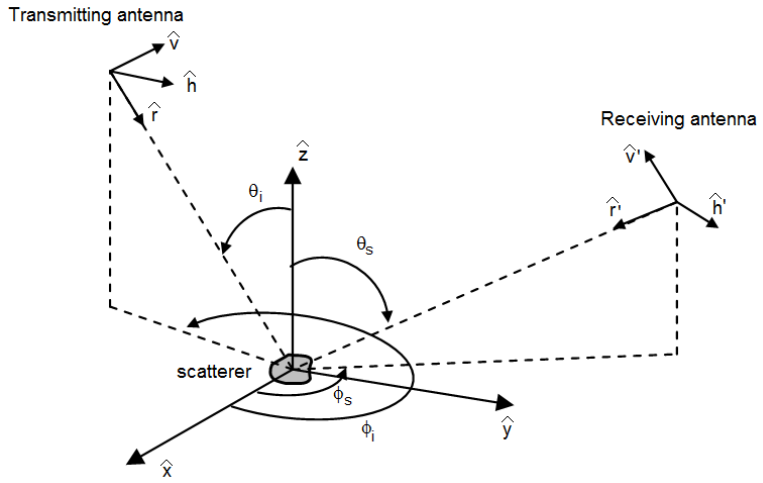

Figure 2.2: Local coordinate systems in Back Scatter alignment (BSA)

radar system with perfect polarization purity and precise alignment of the antennas with respect to an orthogonal reference system. In practical systems, the calibration is required because they may not always reach those ideal conditions and imperfections such as cross-talk between channels or amplitude/phase imbalance in transmitter and receiver may corrupt the measurements.

In our case, the system uses a bistatic configuration, but using the typical model of the monostatic case [11], we can have a schematic block diagram of the measurement system as it is shown in figure 2.3. There, the transmitter (i.e. the satellite) is represented by the block 1. The target of interest is in block 3. Block 2 and 4 are the transmit and receive paths, respectively.

The measurements in 5 are related with the amplitude and phase of the scattered wave. Hence, the scattering properties of the target can be described by a complex polarization matrix $[S]$ [11]. This matrix cannot be measured directly from the target. Instead, the receiver measures the horizontal and vertical components of the electric field, i.e. E_h^r and E_v^r. In the absence of noise, they are related to each other through the measured scattering matrix $[M]$

$$\begin{bmatrix} E_h^r \\ E_v^r \end{bmatrix} = \begin{bmatrix} M_{hh} & M_{hv} \\ M_{vh} & M_{vv} \end{bmatrix} \begin{bmatrix} E_h^t \\ E_v^t \end{bmatrix} \tag{2.1}$$

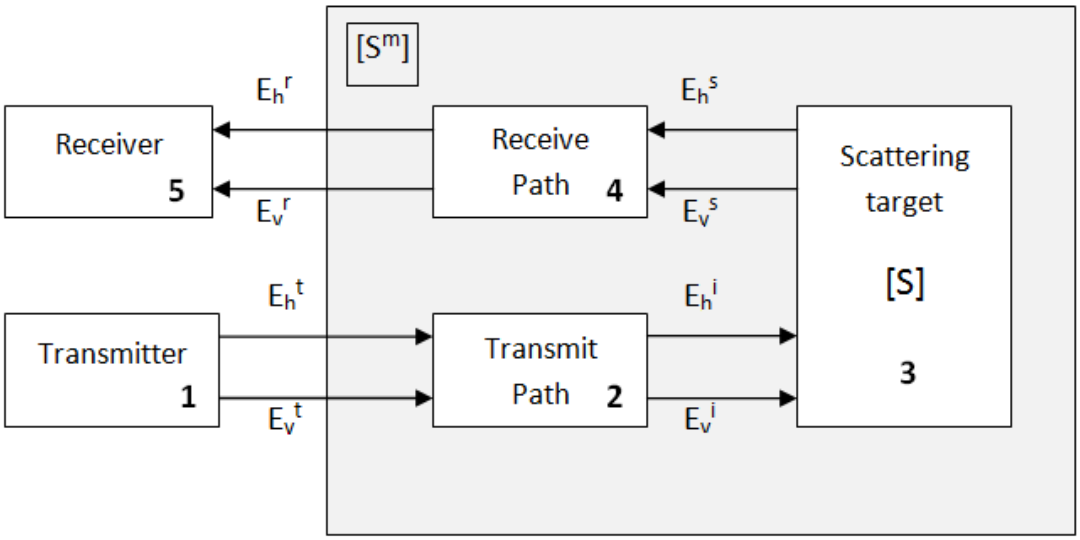

Figure 2.3: Model of measurements in the bistatic sensor of oportunity

2.3.1 Sources of error

Figure 2.3 illustrates the sources of errors that may affect the measurement of the correct scattering matrix of the target. Similarly to the monostatic case [11], in block 1,2,4,and 5 we have errors related to:

- the frequency response of the device
- medium propagation
- channel imbalance
- mismatches in the hardware

Additionally, in block 2 and 4, errors may also be induced by cross-talk in the transmit channels and receive channels, repectively.

From figure 2.3 we can obtain the relationships for the transmitted, incident, scattered, and received waves:

$$\begin{bmatrix} E_h^i \\ E_v^i \end{bmatrix} = [\mathbf{T}] \begin{bmatrix} E_h^t \\ E_v^t \end{bmatrix} \tag{2.2}$$

$$\begin{bmatrix} E_h^s \\ E_v^s \end{bmatrix} = [\mathbf{S}] \begin{bmatrix} E_h^i \\ E_v^i \end{bmatrix} \tag{2.3}$$

$$\begin{bmatrix} E_h^r \\ E_v^r \end{bmatrix} = [\mathbf{R}] \begin{bmatrix} E_h^s \\ E_v^s \end{bmatrix} \tag{2.4}$$

Notice that matrix $[R]$ describes the behavior of the propagation in the path between the target and the receiver, while matrix $[T]$ describes the path between the transmitter and the target. Combining equations 2.2, 2.3 and 2.4, we obtain:

$$\begin{bmatrix} E_h^r \\ E_v^r \end{bmatrix} = [\mathbf{R}]\,[\mathbf{S}]\,[\mathbf{T}] \begin{bmatrix} E_h^t \\ E_v^t \end{bmatrix} \tag{2.5}$$

from equations 2.1 and 2.5, we can identify $[\mathbf{M}]$ as:

$$[\mathbf{M}] = [\mathbf{R}]\,[\mathbf{S}]\,[\mathbf{T}] = \begin{bmatrix} R_{hh} & R_{hv} \\ R_{vh} & R_{vv} \end{bmatrix} \begin{bmatrix} S_{hh} & S_{hv} \\ S_{vh} & S_{vv} \end{bmatrix} \begin{bmatrix} T_{hh} & T_{hv} \\ T_{vh} & T_{vv} \end{bmatrix} \tag{2.6}$$

The measured scattering matrix is in fact a distorted version of the real scattering matrix because the influences of matrices $[R]$ and $[T]$. We can expect to remove the influence of such matrices through a calibration.

2.4 Calibration of the system

Equation 2.6 can also be expressed in terms of vectors by preserving all possible products of R_{ij} and T_{ij} in one matrix.

$$\begin{bmatrix} M_{hh} \\ M_{hv} \\ M_{vh} \\ M_{vv} \end{bmatrix} = \begin{bmatrix} R_{hh}T_{hh} & R_{hh}T_{vh} & R_{hv}T_{hh} & R_{hv}T_{vv} \\ R_{hh}T_{hv} & R_{hh}T_{vv} & R_{hv}T_{hv} & R_{hv}T_{hv} \\ R_{vh}T_{hh} & R_{vh}T_{vh} & R_{vv}T_{hh} & R_{vv}T_{vh} \\ R_{vh}T_{hv} & R_{vh}T_{vv} & R_{vv}T_{hv} & R_{vv}T_{vv} \end{bmatrix} \begin{bmatrix} S_{hh} \\ S_{hv} \\ S_{vh} \\ S_{vv} \end{bmatrix} \tag{2.7a}$$

$$\begin{bmatrix} M_{hh} \\ M_{hv} \\ M_{vh} \\ M_{vv} \end{bmatrix} = \begin{bmatrix} c_{11} & c_{12} & c_{13} & c_{14} \\ c_{21} & c_{22} & c_{23} & c_{24} \\ c_{31} & c_{32} & c_{33} & c_{34} \\ c_{41} & c_{42} & c_{43} & c_{44} \end{bmatrix} \begin{bmatrix} S_{hh} \\ S_{hv} \\ S_{vh} \\ S_{vv} \end{bmatrix} \tag{2.7b}$$

$$\underline{[\mathbf{M}]} = [\mathbf{C}]\,\underline{[\mathbf{S}]} \tag{2.7c}$$

The matrix [**C**] contains all error coefficients inserted in the transmitter and receiver path of the systems, and it is called the *calibration matrix*. We can notice that elements in the diagonal of [**C**] are related with the co-channel radiation while the ones off the diagonal have at least one cross-talk term.

In the ideal case, the transmit and received path would not induce neither errors nor coupling in the channels. Thus, the transmitted fields would be equal to the incidents fields, $E^t_{h,v} = E^i_{h,v}$, and the received fields equal to the scattered ones, $E^r_{h,v} = E^s_{h,v}$. That would imply matrices the $[T]$ and $[R]$ equal to the identity matrix. Consequently, the matrix $[C]$ would become also an identity matrix, and the vector of measurements $\underline{[\mathbf{M}]}$ would be exactly the scattering parameters $\underline{[\mathbf{S}]}$ of the target.

Equation 2.7 leads to a homogeneous system with eight unknown. In monostatic systems, the transmitting and receiving paths can be considered as the same, then reciprocity of the cross-channels reduces the number of unknowns to six. In that case, the system can be solved by using three calibrators with linearly independent scattering matrices [11]. In the bistatic case, the transmissor is in a different location than the receiver. Hence, transmitting and receiving paths are different, and we cannot assume reciprocity of the cross-channels. In this case, we would require four linearly independent calibrators.

In order to simplify the problem, we can make some assumptions regarding the elements in matrix $[C]$. In our particular case, the system presents good cross-polarization isolation (below -30 dB) both in transmission and reception[10, 6]. Thus, the matrix [**C**] can be considered diagonal (equation 2.8) since the magnitud of the cross-talk of [**R**] and [**T**] would be considered negligible with respect to the co-channel terms.

$$\begin{bmatrix} M_{hh} \\ M_{hv} \\ M_{vh} \\ M_{vv} \end{bmatrix} = \begin{bmatrix} c_{11} & 0 & 0 & 0 \\ 0 & c_{22} & 0 & 0 \\ 0 & 0 & c_{33} & 0 \\ 0 & 0 & 0 & c_{44} \end{bmatrix} \begin{bmatrix} S_{hh} \\ S_{hv} \\ S_{vh} \\ S_{vv} \end{bmatrix} \tag{2.8}$$

Notice that from equation 2.8, the coefficients c_{ii} represent a direct relationship between the measurements at the receiver and the scattering coefficients of the target:

$$\tilde{c}_{ii} = \frac{M_{\xi\chi}}{S_{\xi\chi}}, \quad \xi, \chi \in \{h, v\} \tag{2.9}$$

Moreover, these coefficients c_{ii} may be estimated even with one calibrator if all its

scattering parameters are different from zero.

2.5 Retrieving the S-matrix of a target

As depicted in figure 2.3, the receiver is measuring a distorted version of the real target scattering matrix. Calibrators must be used in order to compute the values of the diagonal matrix $[C]$. Clearly, nonzero scattering parameters are required to estimate the corresponding c_{ii} coefficient by using equation 2.9. Then, once we know $\left[\tilde{C}_{target}\right]$, we can retrieve the scattering matrix of the any target by inversion of equation 2.8 :

$$\left[\tilde{S}_{target}\right] = \left[\tilde{C}_{target}\right]^{-1} [M_{target}] \tag{2.10}$$

In the next section, we explore the option of using the *polarimetric active radar calibrators* as control targets in order to estimate the coefficients of the diagonal matrix $\left[\tilde{C}\right]$.

2.6 Conclusions

We can obtain polarimetric measurements by receiving the scattered signal in H and V channel for each H and V polarized pulse from the illuminator of opportunity. RADARSAT-2 offers this possibility since its transmitted signal interleaves vertical and horizontal polarization.

Regarding the scattering matrix of a target, what we measure is a distorted version of the correct one. A model of measurements for the bistatic case was derived from classical monostatic systems. In this model, errors related to the frequency response of the devices, channel imbalance, and mismatches in the hardware are concentrated in the transmitter and receiver. Moreover, errors induced by coupling in the channels and free space propagation are related to the transmit channel and receive channel.

The errors in the measurements can be compensated by means of the calibration matrix $[C]$. This matrix contains the products of co-polar and cross-polar terms of transmit and receive channel. In our approach, $[C]$ was approximated to a diagonal matrix since the system present good polarization isolation. Consequently, the estimation of the calibration coefficients is simplified, and they can be obtained with the ratio of the measurements to the scattering coefficients of the control target. A control target would be enough for the calibration if its scattering matrix has no zero elements.

Chapter 3

PARCs: the calibration targets

PARC (*Polarimetric Active Radar Calibrator*) devices have been effectively use in calibration of monostatic SAR systems and radiometry applications[12, 13]. They are basically *transponders* that receive the RF signal from the radar in one polarization, and they retransmits an amplified version of the signal in other polarization. Figure 3.1(a) depicts the basic PARC's components: two linearly polarized antennas connected to a high-gain RF amplifier.

The use of PARCs offers advantages for experimental campaigns such as compactness of the device, easy deployment, they can have wide beamwidths and high signal-to-background clutter ratio[12]. We have also the possibility of changing the PARC's scattering matrix by rotating each antenna with a different angle. Moreover,for bistatic system, they have the advantage of an independent alignment of each antenna towards the illuminator of opportunity and the sensor. This quality makes easier the computation of their scattering matrices even in field conditions. On the contrast, the hard structure in typical passive reflectors make that the scattering matrix depends utterly on the incidence angle of the wave. This makes them unpractical as bistatic targets outside laboratory conditions.

3.1 Scattering matrices of the PARCs

From the diagram of figure3.1(b), we can obtain a general expression of the scattering matrix of a PARC using unitary vectors of the direction of the electric field [13]. Thus, at the PARC's receiver and transmitter, we have:

$$\hat{e}_r = \sin\alpha\hat{h} + \cos\alpha\hat{v} \tag{3.1}$$

$$\hat{e}_t = \sin\beta\hat{h} + \cos\beta\hat{v} \tag{3.2}$$

Combining equation 3.1 and 3.2, we can obtain a general expression of the matrix [S] of the PARC:

$$[\mathbf{S_{PARC}}] = s_p \begin{bmatrix} \sin\alpha\sin\beta & \cos\alpha\sin\beta \\ \sin\alpha\cos\beta & \cos\alpha\cos\beta \end{bmatrix} \tag{3.3}$$

Where s_p is a complex number which represents the gain and phase introduced by the PARC. In this sense, the magnitude of s_p is related with the RCS of the PARC. Theoretically [14], the effective RCS of a PARC with amplification G_A is given by

$$\sigma_{PARC} = \frac{G_A G^2 \lambda^2}{4\pi} \tag{3.4}$$

where we are assuming that both transmitting and receiving antennas have the same gain G. In addition, the magnitude of the S-parameters are related with the RCS (equation 1.10):

$$\sigma_{PQ} = 4\pi \left|S_{PQ}\right|^2$$

By using equation 3.4 and writing $|s_p|$ in terms of the RCS, it gives

$$|s_p| = \sqrt{\frac{\sigma_{PARC}}{4\pi}} = \sqrt{\frac{G_A G^2 \lambda^2}{(4\pi)^2}} = \frac{G\sqrt{G_A}\lambda}{4\pi} \tag{3.5}$$

In principle, one target (PARC-1) could be enough to know the coefficients c_{ii} of the matrix [**C**] due to the aproximation of having practically zero cross-polar elements. Nevertheless, in the following, we also going to discuss the implementation of the Two-PARC (PARC-2 and PARC-3) configuration in order to know their pros and cons into the calibration process.

First, for the One-PARC configuration, we select the angle of rotation for the receiving and transmiting antenna as $\alpha_1 = \beta_1 = 45\,^\circ$ in PARC-1. Using such values in equation 3.3, the scattering matrix is:

$$[\mathbf{S_1}] = s_{p1}\frac{1}{2}\begin{bmatrix} 1 & 1 \\ 1 & 1 \end{bmatrix} \tag{3.6}$$

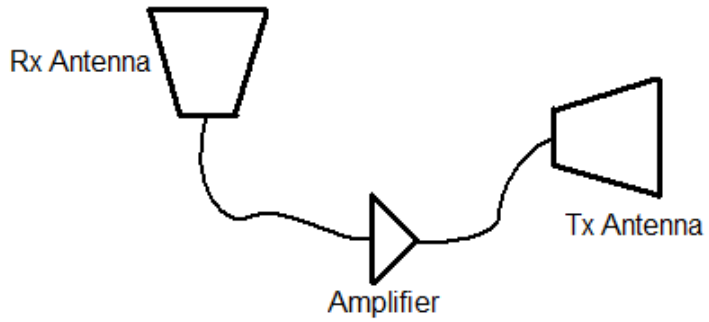

(a)

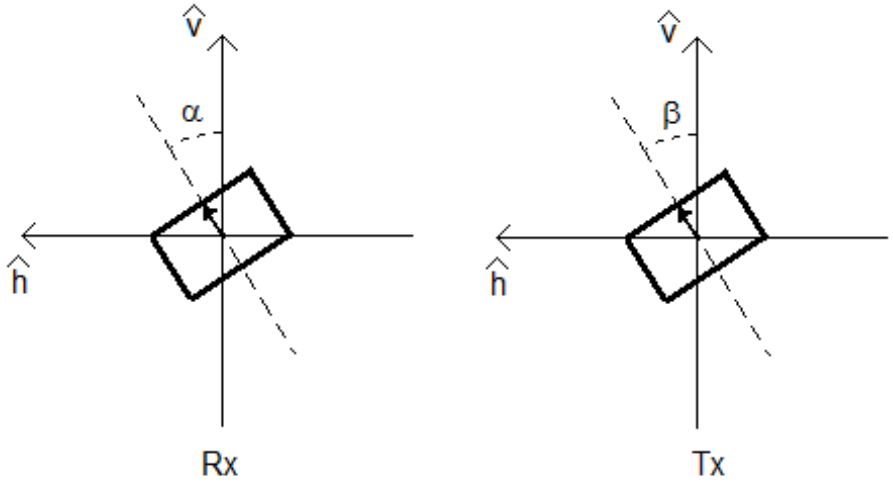

(b)

Figure 3.1: (a) Basic diagram of the PARCs, (b) general case for the antenna positioning of the PARCs

Now, for the Two-PARC configuration, the angles of rotation selected for the receiving and transmiting antenna of PARC-2 are $\alpha_2 = 90\,^\circ$ and $\beta_2 = 45\,^\circ$, respectively. For PARC-3, the angles selected are $\alpha_3 = 0\,^\circ$ and $\beta_3 = 45\,^\circ$. Thus, the resulting scattering matrices are:

$$[\mathbf{S_2}] = s_{p2}\frac{1}{\sqrt{2}}\begin{bmatrix} 1 & 0 \\ 1 & 0 \end{bmatrix} \tag{3.7}$$

$$[\mathbf{S_3}] = s_{p3}\frac{1}{\sqrt{2}}\begin{bmatrix} 0 & 1 \\ 0 & 1 \end{bmatrix} \tag{3.8}$$

Table 3.1 summarizes the characteristics of the One and Two PARC configuration regarding the their scattering matrices.

In the following, for both One-PARC and Two-PARC configuration, we are going to study the impact of alignment errors in obtaining the calibration coefficients and in retrieve the scattering coefficient of a control target. Due to the use of normalized scattering matrices, the variations will be presented as relative errors.

3.2 Alignment errors in One-PARC Configuration

From equarion 2.8,we have described that the estimations of the diagonal elements in $[\mathbf{C}]$ are directly obtained by doing the ratio $\tilde{c}_{ii} = \frac{M_{\xi\chi}}{s_{\xi\chi}}$ (with $\xi, \chi \in \{h, v\}$), and *a priori* knowledge of the scattering parameters $s_{\xi\chi}$ of the PARC is required. However, $[\mathbf{S}]$ would depend on the angles of rotation of the receiving and transmitting antennas (equation 3.3). In this sense, perfect positioning of the PARC is required for a proper calibration. In practice, it could be difficult to place the antennas exactly in their correct positions,

PARC	α	β	Scattering matrix
One-PARC Config: PARC-1	$45\,^\circ$	$45\,^\circ$	$[\mathbf{S_1}] = s_{p1}\frac{1}{2}\begin{bmatrix} 1 & 1 \\ 1 & 1 \end{bmatrix}$
Two-PARC Config: PARC-2	$90\,^\circ$	$45\,^\circ$	$[\mathbf{S_2}] = s_{p2}\frac{1}{\sqrt{2}}\begin{bmatrix} 1 & 0 \\ 1 & 0 \end{bmatrix}$
Two-PARC Config: PARC-3	$0\,^\circ$	$45\,^\circ$	$[\mathbf{S_3}] = s_{p3}\frac{1}{\sqrt{2}}\begin{bmatrix} 0 & 1 \\ 0 & 1 \end{bmatrix}$

Table 3.1: Scattering matrices of PARC-1, PARC-2 and PARC-3

and errors in the $\tilde{c}_{ii}$ coefficients could appear as a consequence of slight variations of α and/or β. In order to analyze the effects of these positioning errors in PARC-1, we introduce the error angles θ and ϕ related to α_1 and β_1, respectively.

$$\alpha_1 = 45^\circ + \theta \tag{3.9}$$

$$\beta_1 = 45^\circ + \phi \tag{3.10}$$

We can express $[\mathbf{S_1}]$ as a function of θ and ϕ by using equation 3.9 and 3.10 into equation 3.3. With the proper trigonometric equivalences, we obtain the effects of such angular error in the S-parameters of PARC-1:

$$[\mathbf{S_1}(\theta,\phi)] = s_{P1}\frac{1}{2}\begin{bmatrix} (\cos\theta+\sin\theta)(\cos\phi+\sin\phi) & (\cos\theta-\sin\theta)(\cos\phi+\sin\phi) \\ (\cos\theta+\sin\theta)(\cos\phi-\sin\phi) & (\cos\theta-\sin\theta)(\cos\phi-\sin\phi) \end{bmatrix} \tag{3.11}$$

Notice that we get the theoretical $[\mathbf{S_1}]$ (equation 3.6) when $\theta = \phi = 0^\circ$.

3.2.1 Simulations

By using the scattering matrix $[\mathbf{S_1}(\theta,\phi)]$, we can obtain the relative errors in the estimation of the coefficients c_{ii} due to the influences of θ and ϕ. For the simulations, we assume a normalized factor $s_{P1} = 1\angle 0^\circ$ and consider $[\mathbf{C}]$ as the identity matrix. Then, we generate the measurements required by adding a (thermal) noise vector $\underline{[N]}$ to 2.8:

$$\underline{[\mathbf{M}]} = [\mathbf{C}]\,\underline{[\mathbf{S_1}(\theta,\phi)]} + \underline{[N]} \tag{3.12}$$

Once we have the vector of measurements, the coefficients of the diagonal matrix $[\mathbf{C}]$ are calculated as:

$$\tilde{c}_{ii} = \frac{M_{\xi\chi}(\theta,\phi)}{s_{\xi\chi}} \tag{3.13}$$

where $M_{\xi\chi}(\theta,\phi)$ represents the measurements obtained in the presence of noise and errors in α_1 and/or β_1, and $s_{\xi\chi}$ is the theoretical value of the scattering coefficient $\xi\chi$ ($\xi,\chi \in \{h,v\}$) of the PARC. One can expect to have only small errors in the alignment of the PARC. Thus, a reasonable range for the values of θ and ϕ is between $\pm 10^\circ$.

Figure 3.2 shows the relative errors of the estimated value $\tilde{c}_{ii}$ respect to the theoretical value c_{ii} for θ and ϕ from -10° to 10°. The behavior of the error has similar

characteristics for the four coefficients $\tilde{c}_{ii}$. For instance, there is diagonal band where the relative error is close to 0% for specific tuples(θ, ϕ). In general, the relative error may no be the same for each coefficient $\tilde{c}_{ii}$, but we found that the relative error in all the cases is less than 6% in the central zone of each image (i.e. $\pm 2\,^\circ$ for θ and ϕ).

Figure 3.3 illustrates the behavior of $\tilde{c}_{ii}$ regarding the relative error for the particular case $\phi = -7\,^\circ$ and different values of θ. In this case, the relative error does not have the same value for all coefficients. For instance, at $\theta = 5\,^\circ$ the relative errors are 5.7%, 20.7%, 20.8% and 1.8% for $\tilde{c}_{11}$, $\tilde{c}_{22}$, $\tilde{c}_{33}$, $\tilde{c}_{44}$, respectively.

As it is depicted in figure 3.2 and 3.3, the relative error in the estimation of c_{ii} is sensitive to variations of both θ and ϕ in the one-PARC configuration, reaching a maximum value around 35% within the range of $\pm 10\,^\circ$.

Errors of the coefficients $\tilde{c}_{ii}$ will propagate in computation of the S-parameters of a target. We can retrieve two of the S-parameters of the PARC-2 in order to show how such errors affects the estimation $\tilde{s}_{\xi\chi}$. Figure 3.4 shows the relative errors in $\tilde{s}_{hh}$ and $\tilde{s}_{vh}$ of the scattering matrix of PARC-2 (equation 3.7). The maximum relative error for any combination (θ, ϕ) is 52% in the interval between $\pm 10\,^\circ$ for both $\tilde{s}_{hh}$ and $\tilde{s}_{vh}$. Nevertheless, for small angular variations (e.g. between $\pm 3\,^\circ$) the relative error does not exceed 11%.

Regarding possible changes in the phase of the coefficients, we see that the coefficients of $[\mathbf{S_1}\,(\theta, \phi)]$ (equation 3.11) do not present any change of sign in the range considered for θ and ϕ (much less than $45\,^\circ$). Consequently, angular errors affect only the magnitude of each $\tilde{c}_{ii}$. Thus, the estimation of the phase of a target's S-parameters will not be affected neither by the angular error θ nor ϕ.

3.3 Alignment errors in Two-PARC Configuration

In this configuration each PARC provides two scattering parameters for the estimation of their corresponding $\tilde{c}_{ii}$. For instance, only the firs column of $[\mathbf{S_2}\,(\theta, \phi)]$ will be use for the estimation of the coefficients c_{11} and c_{33} in $[\mathbf{C}]$ when receiving horizontal polarized waves from the satellite. Similarly, only the second column of $[\mathbf{S_3}\,(\theta, \phi)]$ would be used to estimate the other two coefficients of $[\mathbf{C}]$ when receiving vertical polarized waves. Since we can consider that the errors in a pair of coefficients $\tilde{c}_{ii}$ are independent from the other pair, we will focus the following procedure to the PARC-2 - the conclusions obtained would be applicable for PARC-3 as well. We follow an analogous methodology

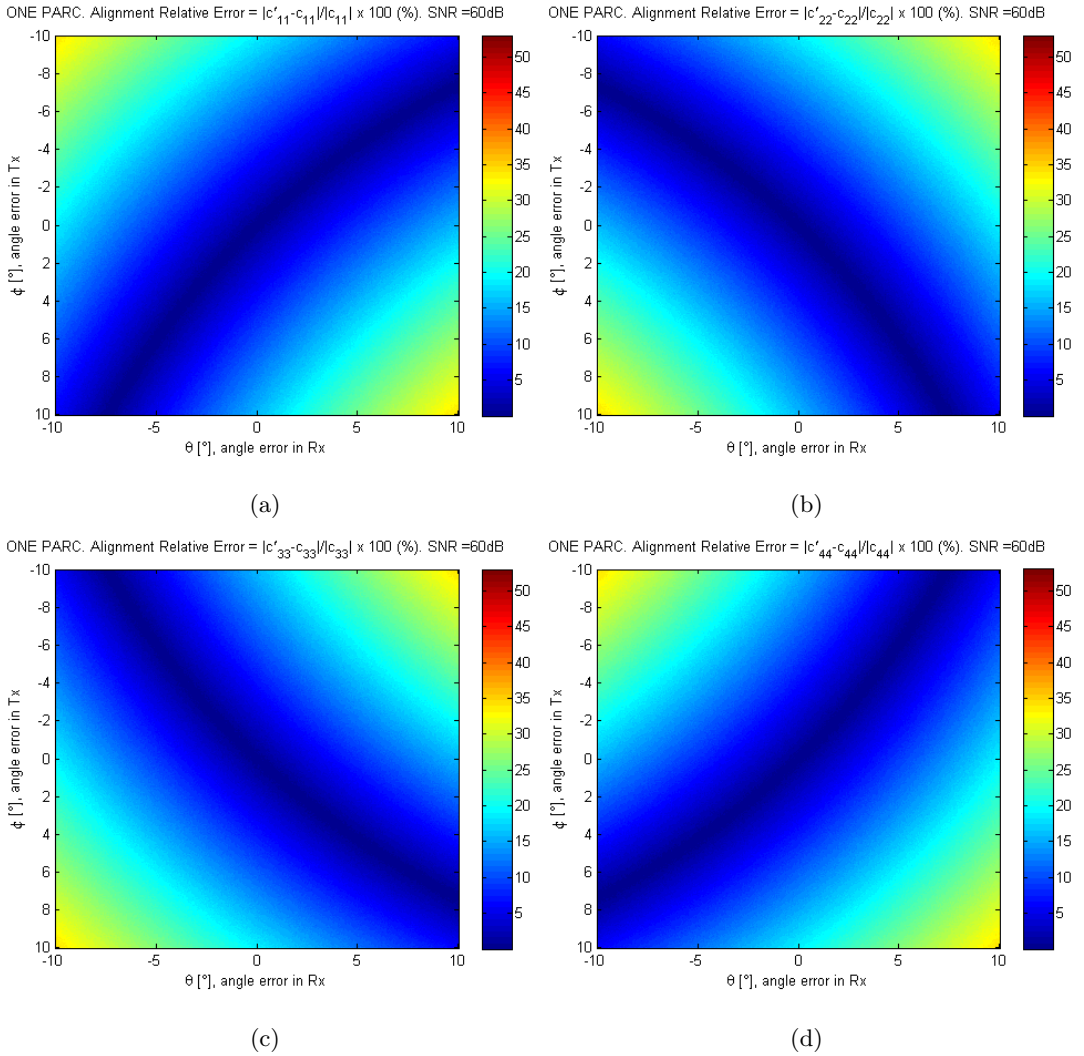

Figure 3.2: Relative error (%) of the estimated values of [C] as a function of θ and ϕ for the One-PARC configuration. a) $\tilde{c}_{11}$, b) $\tilde{c}_{22}$, c) $\tilde{c}_{33}$, d) $\tilde{c}_{44}$. SNR = 60 dB

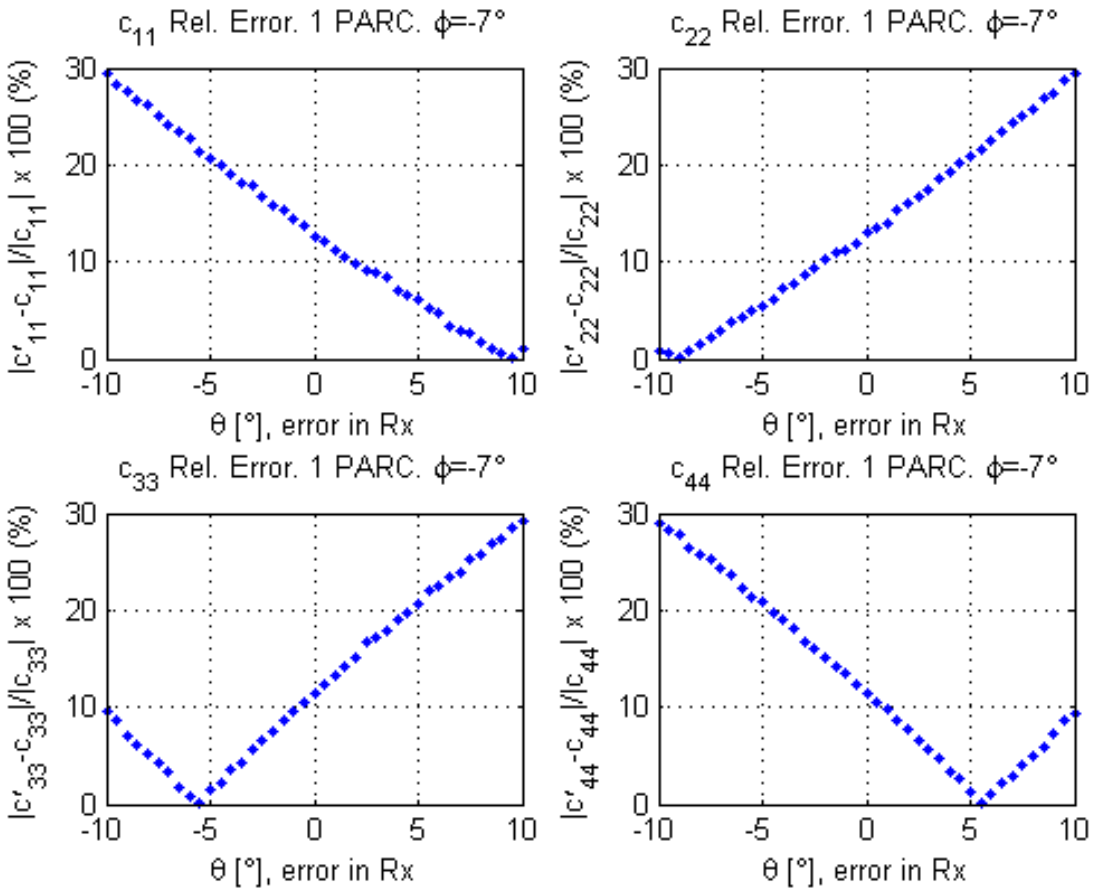

Figure 3.3: Relative errors of the coefficients $\tilde{c}_{ii}$ for $\phi = -7^\circ$ and θ between $\pm 10^\circ$. SNR = 60dB

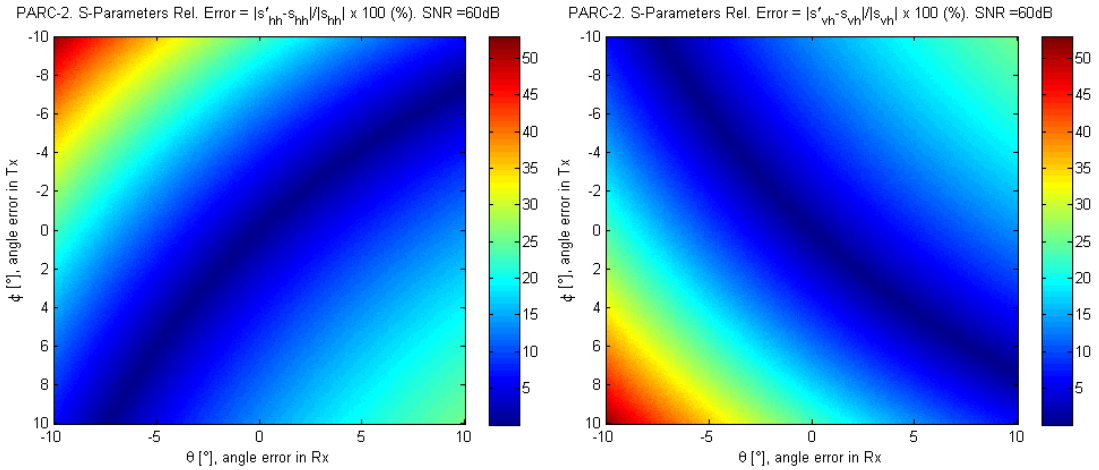

(a) (b)

Figure 3.4: Relative errors (%) of coefficients from the scattering matrix of PARC-2. (a)$\tilde{s}_{hh}$ and (b)$\tilde{s}_{hh}$ as functions of θ and ϕ. SNR = 60dB

than in the case of One-PARC configuration by using the same error angles θ and ϕ:

$$\alpha_2 = 90\,^\circ + \theta \tag{3.14}$$

$$\beta_2 = 45\,^\circ + \phi \tag{3.15}$$

If we use equations 3.14 and 3.15 into equation 3.3, we obtain:

$$[\mathbf{S_2}\,(\theta,\phi)] = s_{P2}\frac{1}{\sqrt{2}}\begin{bmatrix} (\cos\theta)\,(\cos\phi+\sin\phi) & (-\sin\theta)\,(\cos\phi+\sin\phi) \\ (\cos\theta)\,(\cos\phi-\sin\phi) & (-\sin\theta)\,(\cos\phi-\sin\phi) \end{bmatrix} \tag{3.16}$$

The four scattering coefficients in equation 3.16 are also functions of θ and ϕ like in the One-PARC configuration. However, in this case the first column of $[\mathbf{S_2}\,(\theta,\phi)]$ has dependency on θ only through its cosine. It is expected less sensitivity of the relative error respect to variations of θ since $\cos\theta \sim 1$ if θ remains small, which is the case of most of the values in the range between $\pm 10\,^\circ$. For ϕ, it is expected to obtain a similar behavior of relative error than the case of One-PARC configuration because we find the same addition and subtraction of sinus and cosines in the scattering parameters.

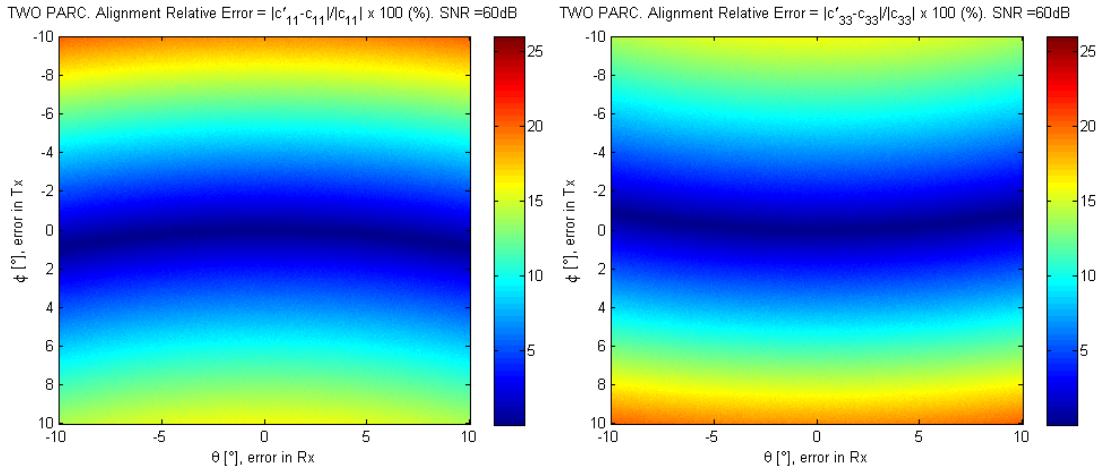

(a) (b)

Figure 3.5: Relative error (%) of the estimated values of [**C**] as a function of θ and ϕ for the case of Two-PARC configuration. a) $\tilde{c}_{11}$, b) $\tilde{c}_{33}$. SNR = 60 dB

3.3.1 Simulations

The measurements and estimations are generated with the same assumptions as for the One-PARC configuration. The only difference is that in this case the computations are just for the two corresponding scattering coefficients of the PARC-2, i.e. s_{hh} and s_{vh}.

Figure 3.5 depicts the behavior of the relative error in $\tilde{c}_{11}$ and $\tilde{c}_{33}$ while varying θ and ϕ. Same results would be obtained for $\tilde{c}_{22}$ and $\tilde{c}_{44}$. The relative error of both $\tilde{c}_{11}$ and $\tilde{c}_{33}$ presents symmetry and small variations along the θ axis. For instance, for $\phi = 0\,°$(figure 3.6(a)), the relative error of $\tilde{c}_{11}$ remains within 0% and 1.7%. On the other hand, it is observed larger variations of the relative error for the same estimation at the different values of ϕ. Figure 3.6(b) illustrates how the relative error of $\tilde{c}_{11}$ varies with $\theta = 0\,°$, presenting a maximum value of 19%. We found similar characteristics in the case of $\tilde{c}_{33}$.

The two-PARC configuration has the advantage of providing estimations $\tilde{c}_{ii}$ less sensible to errors regarding the alignment of the receiving antenna (i.e. the antenna that is pointing the satellite), which in practice may presents more difficulties in achieving a perfect positining. Nevertheless, the alignment of the transmitting antenna presents the same error sensitivity than the One-PARC configuration.

We can retrieve now two of the S-parameters of the PARC-1 in order to show how

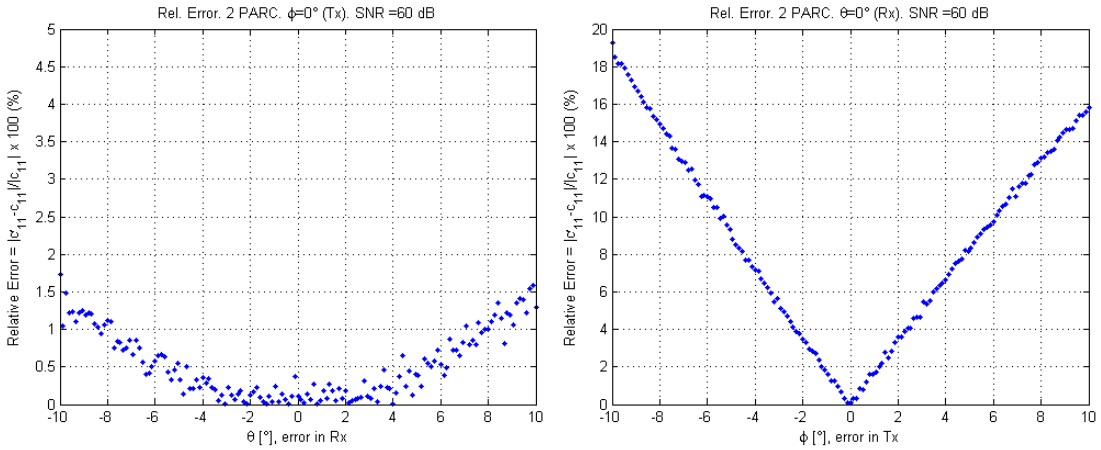

(a) (b)

Figure 3.6: Relative error (%) of $\tilde{c}_{11}$ in Two-PARC configuration, a) function of $\theta(\phi = 0\,^\circ)$, b) function of $phi(\theta = 0\,^\circ)$. SNR =60 dB.

the errors in $\tilde{c}_{11}$ affects the estimation $\tilde{s}_{\xi\chi}$. Figure 3.7 depicts the relative errors in the parameters $\tilde{s}_{hh}$ and $\tilde{s}_{vh}$ of the scattering matrix of PARC-1. In this case, the maximum error for any combination (θ, ϕ) in the interval between $\pm 10\,^\circ$ is 25% for $\tilde{s}_{hh}$ and $\tilde{s}_{vh}$. If we have small angular variations (e.g. around $\pm 3\,^\circ$) the relative error decrease significantly and it is less than6%. Thus, the Two-PARCs configuration is more robust against errors in the positioning of the antennas than the One-PARC configuration.

Similarly to the One-PARC configuration, the coefficients of $[\mathbf{S_2}\,(\theta, \phi)]$ used in obtaining $\tilde{s}_{hh}$ and $\tilde{s}_{vh}$ do not present any change of sign within the range of values of θ or ϕ. The phase of each $\tilde{c}_{ii}$ coefficient is not affected by small angular variations in the positioning of the antennas, and these errors will be only reflected in the estimation of the magnitude of a target's S-parameters.

3.4 Influence of the amplitude and phase response of the PARCs

In previous sections, we had considered that the amplification and phase introduced by the PARC are well known in the estimation $\left[\tilde{\mathbf{C}}\right]$, which is part of the ideal case in retrieving the S-parameters of a targe of interest. In practice, we may find different responses from each PARC. Moreover, even if we knew exactly the phase due to the

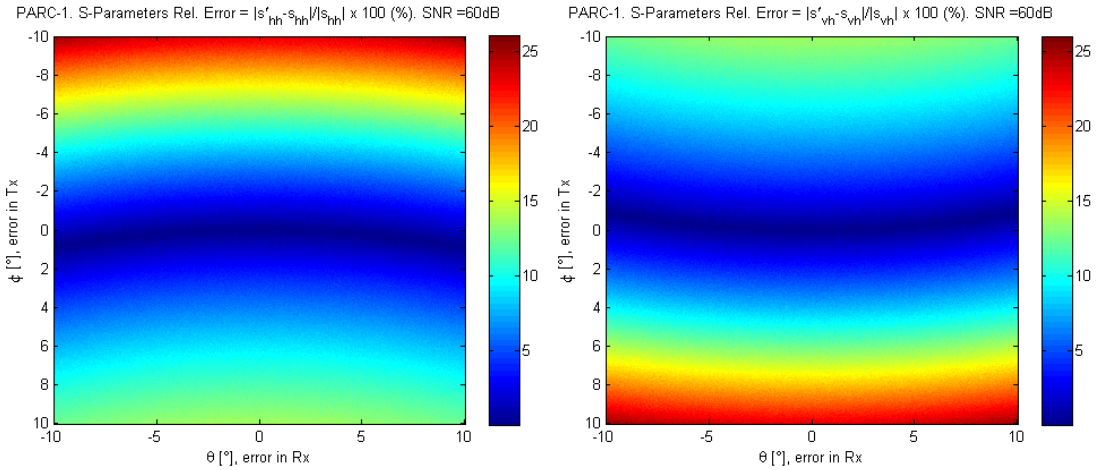

(a) (b)

Figure 3.7: Relative errors (%) in (a)$\tilde{s}_{hh}$ and (b)$\tilde{s}_{vh}$ of the scattering matrix of PARC-1 as function of θ and ϕ. SNR = 60dB.

device itself, the phase of the signal may be particularly difficult to estimate in field experiments because we may not have an accurate measurement of the distance (in terms of the wavelength) between the satellite and each of the PARCs, and between the latter and the sensor. Nevertheless, it is required to characterize the PARCs to have the best approximation of coefficients of the real matrix $[\mathbf{C}]$, and consequently, a correct estimation of the S-parameters of any target.

In this section, we will assume perfect alignment of the antennas (i.e. $\theta = \phi = 0\,^\circ$) and we introduce the parameters A and γ in order to consider the variations in amplitude and phase, respectively. In particular, γ is composed as $\gamma = -\delta_{P1} + k\,(r_{sat} + r_{sen})$, where δ_P represents a phase introduced by the PARC itself, k the wavenumber, r_{sat} the distance from the satellite to the PARC's receiver and r_{sen} the distance from the PARC's transmitter to the sensor. We will work only with γ representing the phase obtained from the contribution of all the factors. Thus, for a given scattering matrix of a PARC, we have:

$$[\mathbf{S_{PARC}}\,(\mathbf{A}, \gamma)] = Ae^{-j\gamma} s_P\,[\mathbf{S}] \tag{3.17}$$

The coefficients $\tilde{c}_{ii}$ would be also function of those two parameters:

$$\tilde{c}_{ii}\left(A,\gamma\right)=\frac{M_{\xi\chi}\left(A,\gamma\right)}{s_{\xi\chi}},\quad \xi,\chi\in\{h,v\} \tag{3.18}$$

3.4.1 One-PARC Configuration

For this configuration, the error parameters A_1 and γ_1 are common for the estimation of the four $\tilde{c}_{ii}$ coefficients since we only have one PARC. Then, from equation 3.17 and 3.13 we have:

$$\tilde{c}_{ii}\left(A_1,\gamma_1\right)=\frac{M_{\xi\chi}}{s_{\xi\chi}A_1e^{-j\gamma_1}}=\tilde{c}_{ii}\frac{1}{A_1}e^{j\gamma_1} \tag{3.19}$$

Thus, the scattering parameters of any target would be retrived as:

$$\underline{[\mathbf{S_{target}}]}=A_1e^{-j\gamma_1}\left[\tilde{\mathbf{C}}\right]^{-1}\underline{[\mathbf{M_{target}}]} \tag{3.20}$$

we observe from equation 3.20 that the errors are present as a common complex number multiplying the matrix $\left[\tilde{\mathbf{C}}\right]$. Consequently, all the estimated S-parameters of the target will have the same offset.

The PARC-2 is used as target in order to show the influence of the error $A_1e^{-j\gamma_1}$ in the estimation of the magnitude and phase of its theoretical S-parameters. Additionally, we assume $s_{P2}=1\angle 0\,^\circ$ and no positioning errors. Figure 3.8 shows the magnitude of the parameters $\tilde{s}_{hh}$ and $\tilde{s}_{hv}$ retrieved from the target considering only the amplitude errors ($\gamma_1=0$) varying A_1 from -10 dB to 10dB. The green line in the figure denotes the theoretical magnitude of the respective S-parameter. Figure 3.9 shows the phase retrieved for the $\tilde{s}_{hh}$ and $\tilde{s}_{hv}$ parameters of the same target. In this case, $A_1=0$ dB and γ_1 varies from $-\pi$ to $+\pi$. The error γ_1 is affecting directly the phase of $\tilde{s}_{hh}$. For the particular case of having PARC-2 as a target, the results for the phase of $\tilde{s}_{hv}$ (and $\tilde{s}_{vv}$) are not reliable since its magnitude is practically zero, as shown in figure 3.8(a).

In applications such as polarimetry [2], the products $s_{\zeta\xi}\cdot s^*_{\chi\psi}$ (with $\zeta,\xi,\chi,\psi\in\{h,v\}$ in the covariance matrix require perfect knowledge of the scattering matrix of the target. Errors in the estimation of the coefficients $\tilde{c}_{ii}$ would lead to errors in the covariance matrix. In the case of the One-PARC configuration, the products $s_{\zeta\xi}\cdot s_{\chi\psi}*$ are modified only by the error parameter A_1 since all S-parameters would have the same error γ_1 in phase:

$$s_{\zeta\xi}\left(A_1,\gamma_1\right)\cdot s_{\chi\psi}\left(A_1,\gamma_1\right)^*=A_1^2s_{\zeta\xi}\cdot s^*_{\chi\psi} \tag{3.21}$$

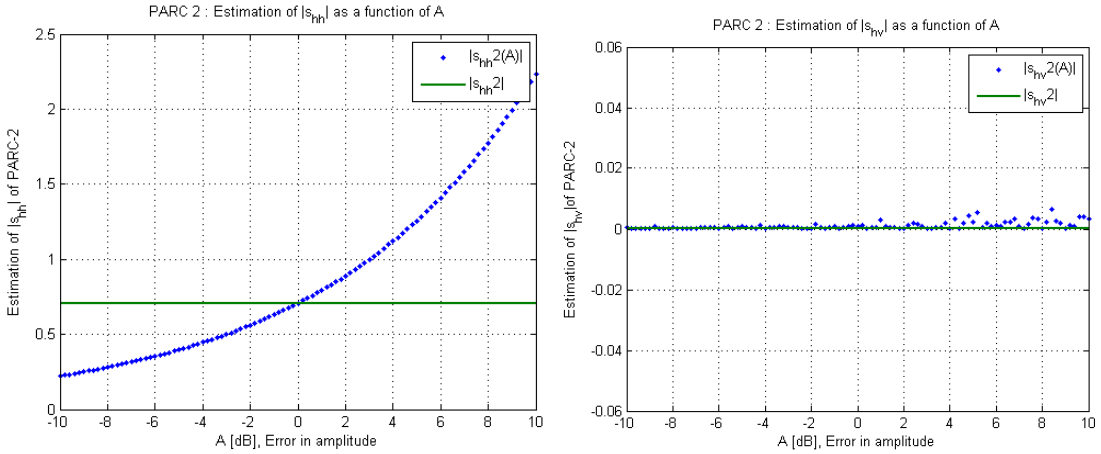

(a) (b)

Figure 3.8: Magnitude of two S-parameters retrieved from PARC-2 (target) as a function of A_1; a)$\tilde{s}_{hh}$, b)$\tilde{s}_{hv}$. SNR =60dB

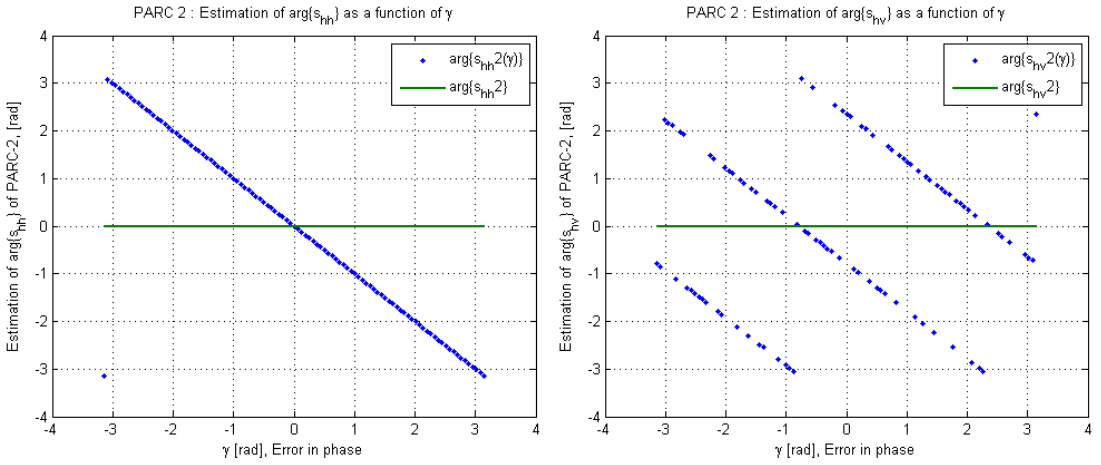

(a) (b)

Figure 3.9: Phase of two S-parameters retrieved from PARC-2 (target) as a function of γ_1; a)$\tilde{s}_{hh}$, b)$\tilde{s}_{hv}$. SNR =60dB

3.4.2 Two-PARC Configuration

In an analogous way to the One-PARC configuration, we use the parameters A and γ related to errors in amplitude and phase, respectively, of the correct S-parameters of $[\mathbf{S_{2,3}}]$. In the case of the Two-PARC configuration, we will have (A_2, γ_2) for PARC-2 and (A_3, γ_3) for PARC-3. Here, we are considering that each PARC may present different errors, and then:

$$\tilde{c}_{11,33}\left(A_{11,33}, \gamma_{11,33}\right) = \frac{M_{11,33}}{s_{11,33}A_{11,33}e^{-j\gamma_{11,33}}} = \tilde{c}_{11,33}\frac{1}{A_{11,33}}e^{j\gamma_{11,33}} \tag{3.22}$$

$$\tilde{c}_{22,44}\left(A_{22,44}, \gamma_{22,44}\right) = \frac{M_{22,44}}{s_{22,44}A_{22,44}e^{-j\gamma_{22,44}}} = \tilde{c}_{22,44}\frac{1}{A_{22,44}}e^{j\gamma_{22,44}} \tag{3.23}$$

The PARC-1 is now used as target in order to show the influence of the parameter $A_2e^{-j\gamma_2}$ in the estimation of the scattering matrix shown in equation 3.6. It is also assumed $s_{P1} = 1\angle 0\,^\circ$ and no positioning errors. Figure 3.10(a) depicts the magnitude retrieved for the $\tilde{s}_{hh}$ of the target (PARC-1) considering variation of A_2 from -10 dB to 10dB, while figure 3.10(b) shows the phase retrieved for the same s-parameter when γ_2 varies from $-\pi$ to $+\pi$. Since the four S-parameters for PARC-1 are the same, the results shown for $\tilde{s}_{hh}$ are applicable for $\tilde{s}_{hv}$, $\tilde{s}_{vh}$ and $\tilde{s}_{vv}$. Once more, in these figures,the green line denotes the correct magnitude and phase of s_{hh}, while the blue dots are the estimations $\tilde{s}_{hh}\left(A_2, \gamma_2\right)$.

The results in the previous charts have similar behavior than the case of One-PARC configuration. Nevertheless, there is no longer a common complex number that multiplies the matrix $[\mathbf{C}]$ unless both PARCs were equal, which is the ideal case. If we consider polarimetry applications, differences between the responses of the PARCs will modify both magnitude and phase of the products $s_{\zeta\xi} \cdot s^*_{\chi\psi}$ (with $\zeta, \xi, \chi, \psi \in \{h, v\}$ required to obtain the covariance matrix. Moreover, not all products would be affected in the same manner because each pair of the s-parameters is estimated through different PARCs. Thus, we have that $s_{hh}\left(A_2, \gamma_2\right)$ and $s_{vh}\left(A_2, \gamma_2\right)$ are related to PARC-2, while $s_{vh}\left(A_3, \gamma_3\right)$ and $s_{vv}\left(A_3, \gamma_3\right)$ are related to PARC-3.

For the S-parameters related to the same PARC, only the magnitude of the product $s_{\zeta\xi} \cdot s^*_{\chi\psi}$ is modified:

$$s_{\zeta\xi}\left(A_{2,3}, \gamma_{2,3}\right) \cdot s_{\chi\psi}\left(A_{2,3}, \gamma_{2,3}\right)^* = A^2_{2,3}s_{\zeta\xi} \cdot s^*_{\chi\psi} \tag{3.24}$$

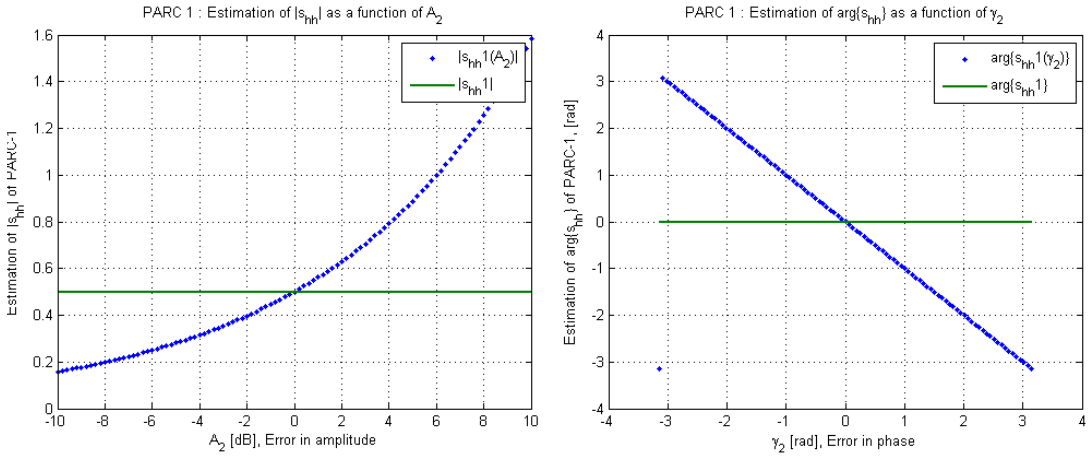

(a) (b)

Figure 3.10: Estimation of of PARC-1's s_{hh} (target), a) magnitud as a function of A_2, b)phase as a function of γ_2. SNR =60dB

In the case of doing $s_{\zeta\xi} \cdot s^*_{\chi\psi}$ among s-parameters estimated from different PARCs, in general, the products will be modified in magnitude and phase:

$$s_{\zeta\xi}\left(A_2, \gamma_2\right) \cdot s_{\chi\psi}\left(A_3, \gamma_3\right)^* = A_2 A_3 e^{j(\gamma_2 - \gamma 3)} s_{\zeta\xi} \cdot s^*_{\chi\psi} \tag{3.25}$$

or

$$s_{\zeta\xi}\left(A_3, \gamma_3\right) \cdot s_{\chi\psi}\left(A_2, \gamma_2\right)^* = A_3 A_2 e^{j(\gamma_3 - \gamma 2)} s_{\zeta\xi} \cdot s^*_{\chi\psi} \tag{3.26}$$

Both products at equations 3.25 and 3.26 are dependent of the differences of the phase introduced by each PARC itself and by their physical placing in the testing field.

3.5 Conclusions

The PARCs have the advantage of providing several scattering matrices according to the position of their receiving and transmitting antennas. Thus, they can be used for calibration of both co-polar and cross-polar terms. Moreover, they can have high amplification of the signal, and their wide beamwidth make easy point to the transmitter and detector. Additionally, their compactness makes them suitable for transportation.

PARCs have many advantages respect to passive devices, but one of their main drawback is their sensitivity to errors in the alignment of the antennas. From the

two configurations discussed for calibration, the One-PARC configuration had higher sensitivity with respect to positioning errors. It was also observed that its relative error was not symmetrical and that it may be cancelled for certain combination of errors. In this configuration, if the PARC is not well characterized, the calibrated measurements would have the same offset in amplitude and phase.

In the range of $\pm 10\,^{\circ}$, the Two-PARC configuration is more robust against errors in the alignment of the receiving antenna. However, it is required a perfect characterization of the PARCs in order to obtain balanced channels after calibration since each PARC is used to calibrate two of the scattering coefficients of any target.

Considering only the alignment of the antennas, if we keep the alignment errors of the antennas between $\pm 3\,^{\circ}$, the relative errors in the estimation of a target's S-matrix would not exceed 11% in the One-PARC configuration, and 6% in the Two-PARC configuration.

Chapter 4

Experimental Campaing

4.1 RADARSAT-2

The RADARSAT-2 satellite carries a synthetic aperture radar (SAR) system for commercial earth observation applications[10]. Moreover, it is capable of polarimetric measurements by interleaving H and V polarized pulse transmissions and receiving simultaneous in H and V. Table 4.1 shows details regarding RADARSAT-2's orbit and characteristics of its transmitted signal.

In our case, the SAR sensor uses RADARSAT-2's transmission as signal of opportunity in order to perform also polarimetric measurements. Thus, the sensor was adapted to measure the scattered fields through four channels: two in H, and two in V. The aim of deploying such configuration is recording data further PolSAR and InPolSAR processing. Moreover, another channel is required to register the direct signal from the satellite to be able to identify the echoes of the respective H and V transmitted polarization signals. Figure 4.1(a) shows the pulses from the direct signal. The antenna of the direct path was tilted ($\sim 60\,^{\circ}$) in order to distinguish H and V pulses by means of their amplitude.

Currently, the SABRINA has only four available channels (figure 4.1(b)). Hence, signals from the scattered path are mixed with the signal of the direct path in one of the channels. At the data processing stage, such signals are split again to create virtually the fifth channel for the direct signal.

RADARSAT-2 Orbit Parameters	
Inclination	98.6 °
Altitude	798 km
Orbits per day	14.3
Repeat cycle	24 days
Sensor Electronics subsystem	
Radar Frequency	5405MHz
PRF	1000Hz or 3800Hz
Pulse length	21μ s or $42\mu s$
Standard pulse bandwidth	$11.56, 17.28, 30.0, 50.0$ MHz
Standard pulse waveforms	Linear FM (up or down chirp)

Table 4.1: RADARSAT-2: general characteristics of its orbit and transmitted signal.

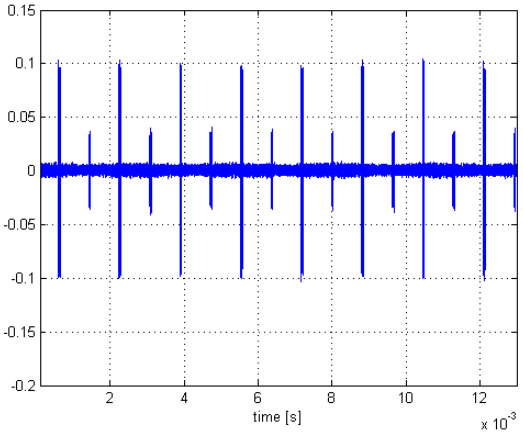

(a)

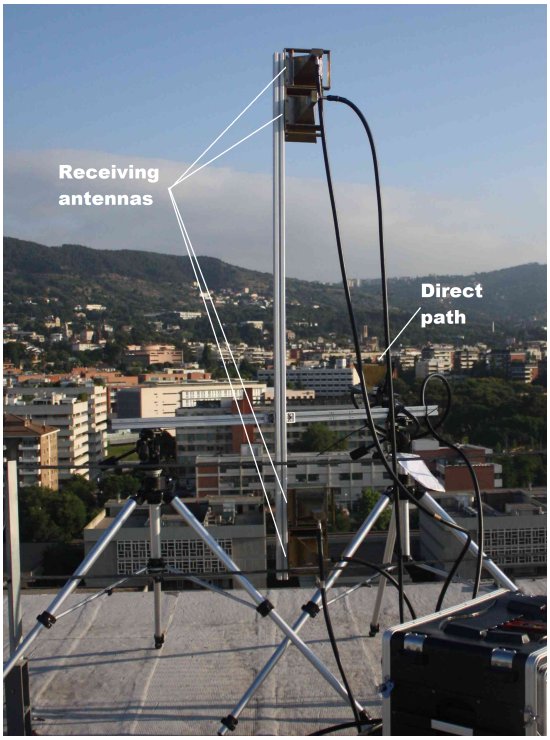

(b)

Figure 4.1: a) Interleaved H and V pulses from RADARSAT-2 transmitted signal. Pulses with larger amplitude correspond to the V polarization. b) SABRINA system

4.2 PARC implementation

4.2.1 Structure

As it was stated in chapter 3, the PARCs may have different scattering matrices depending on the angle of rotation of each antenna. We have also studied two different configurations: the first one is using only one PARC, while the second one has two PARCs. Figure 4.2 depicts each of those configurations

Either the One-PARC or Two-PARC configuration requires a physical structure capable of withstanding the weight of the antenna array while providing a degree of freedom for angular adjustments of each antenna. Moreover, since the PARCs are planned to be used in outdoor experimental campaigns, they must be easy to transport, deploy, and be adaptable to the terrain's conditions.

In order to fulfill the previous requirements, the structure selected for the prototype PARCs is based on tripods. The One-PARC configurations requires both transmitting and receiving antennas to be rotated $\alpha = \beta = 45\,^\circ$ with respect to the vertical axis (figure 4.2). In practice, the main challenge of this configuration comes from pointing the receiver antenna to the passing of RADARSAT-2. We have to put the antenna at large elevation angles ($\sim 62\,^\circ$) and, at the same time, with a $45\,^\circ$ rotation. For the transmitting antenna, the positioning is easier since we have line-of-sight with the detector.

The Two-PARC configuration presents less sensibility to alignment errors at the receiving antennas. Hence, we can relax the accuracy required in their positioning. Moreover, the positioning of the receiving antenna is easier in this case because once we put the antenna in vertical or horizontal polarization, we only have to tilt it with the correct elevation angle. For each PARC, we mounted both antennas on the same structure, using angle-locking brackets to tilt the antennas in elevation for the reception and $45\,^\circ$ rotation for transmission(figure 4.3). All the structure is placed on one tripod whose legs can be slightly adjusted (if necessary) to achieve the (small) elevation angle for transmitting to the SAR detector.

4.2.2 PARCs' antennas

The antennas used in the implementation of the PARCs are linear polarized horn antennas for C-Band. Figure 4.4 shows their physical dimensions.

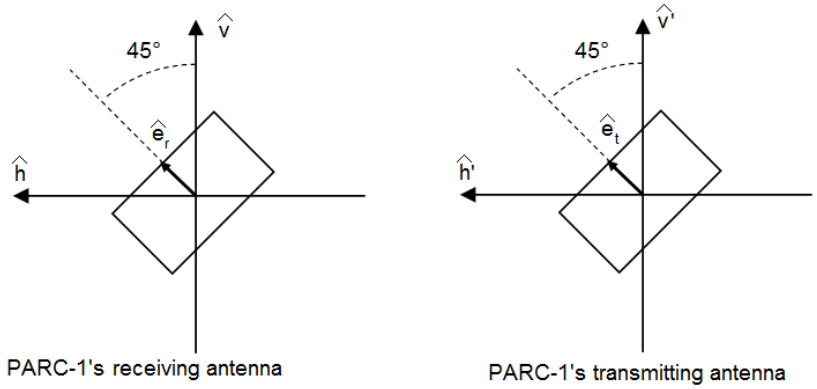

(a)

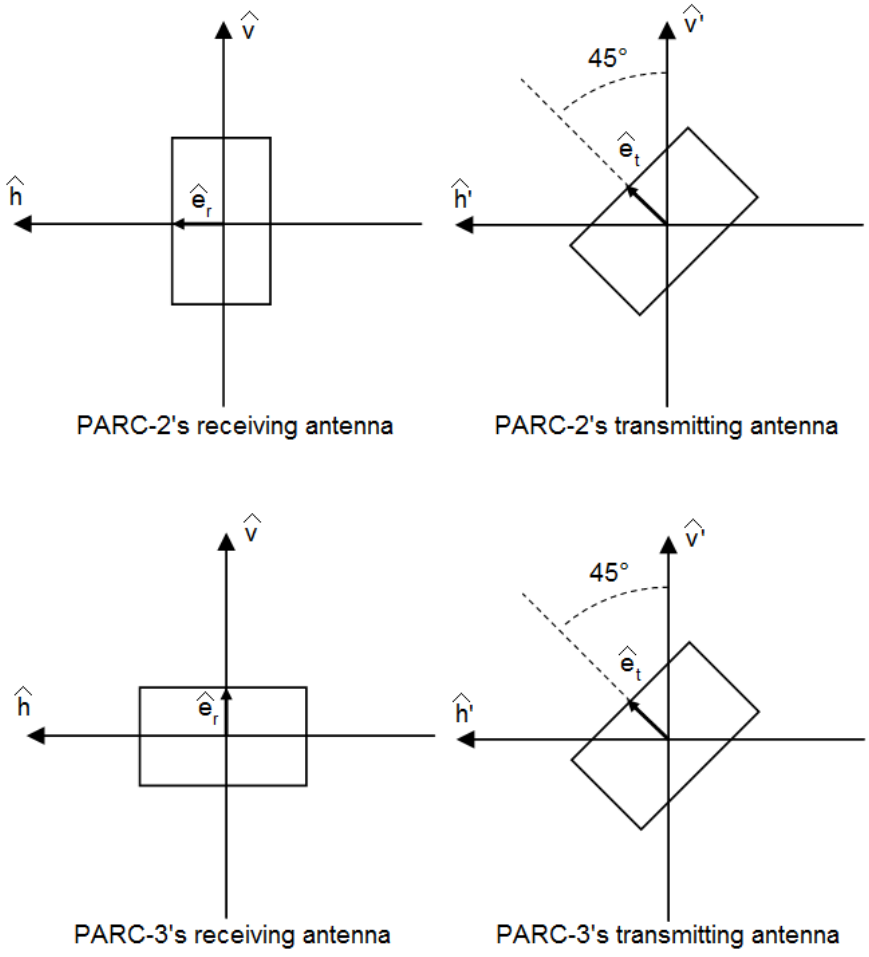

(b)

Figure 4.2: PARC configuration for calibration: a) One-PARC configuration, b) Two-PARC configuration.

Figure 4.3: Prototype of the structure for the PARCs.

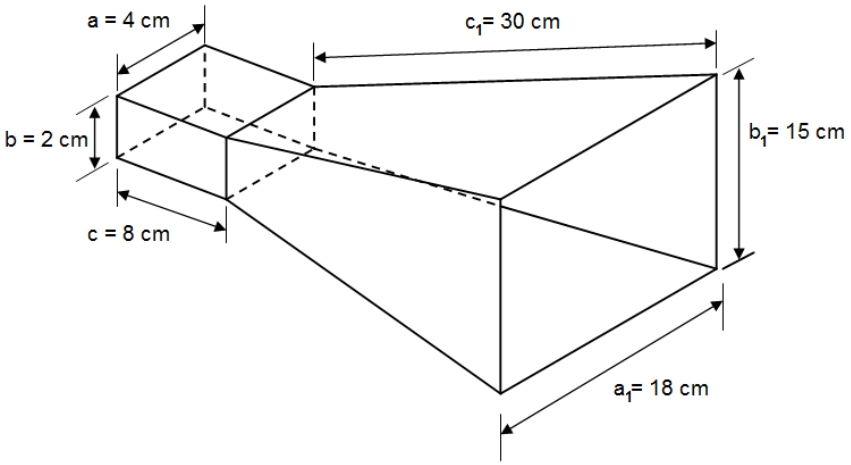

Figure 4.4: Physical dimensions of the linear polarized horn antenna.

The antennas has a beamwidth of 20 ° at E and H planes and a directivity of 16 dB[15]. Figure 4.5(c) shows the measured radiation pattern at 5.405 GHz, while figure 4.5(a) and 4.5(b) show the radiation pattern in E and H planes, respectively, for 5.3 GHz, 5.4 GHz and 5.5 GHz.

4.2.3 Amplifiers

Each PARC has a C-Band amplifier between the two horn antennas. Figure 4.6 shows the magnitude their parameters S_{11}, S_{22}, and S_{21}. At RADARSAT-2 operating frequency (5.405 GHz), each amplifier provides +31.9dB, +32.8dB and +18.2dB. Each of the $\sim$ 32dB amplifiers contains two amplifiers *mini-circuit* model ZX60-5916M connected in series. The other is a single amplifier *MIMIX* model CGB7014.

Influence of the temperature

Temperature may change the frequency response of the amplifiers. They were measured in the climatic chamber from 5 °C to 35 °C with a 10 °C step. Figure 4.7 shows the changes in magnitude and phase of parameter S_{21} of amplifier 1.

For RADARSAT-2's operating frequency, figure 4.8 shows the magnitude and phase of S_{21} of the amplifier 1 as a function of the temperature. Similar behavior is presented in amplifier-2 and amplifier-3(appendix A.1). Assuming that such variations in S_{21} can be represented by a first order polynomial, we have the following expression:

$$|S_{21}(T)|_{amplif-1} = -0.0383T + 32.8636\,[\text{dB}] \tag{4.1}$$

$$Arg\{S_{21}(T)\}_{amplif-1} = 0.3896T - 111.7935\,[^\circ] \tag{4.2}$$

Similarly, for the amplifier 2 we have:

$$|S_{21}(T)|_{amplif-2} = -0.0315T + 33.5954\,[\text{dB}] \tag{4.3}$$

$$Arg\{S_{21}(T)\}_{amplif-2} = 0.4742T - 110.8489\,[^\circ] \tag{4.4}$$

And for the amplifier 3:

$$|S_{21}(T)|_{amplif-3} = -0.0213T + 18.7417\,[\text{dB}] \tag{4.5}$$

$$Arg\{S_{21}(T)\}_{amplif-3} = 0.5816T - 71.3936\,[^\circ] \tag{4.6}$$

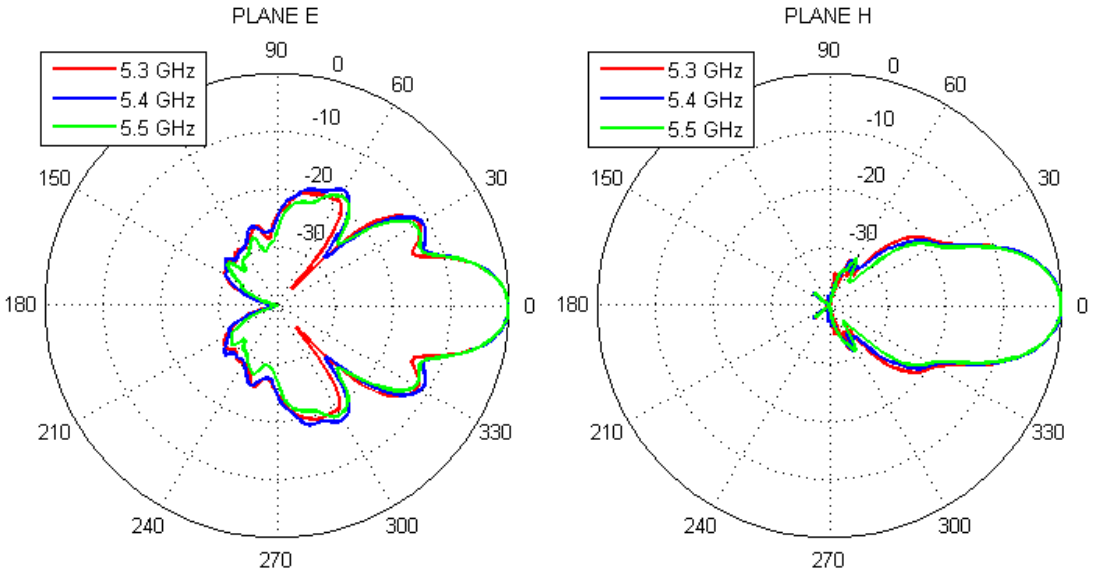

(a) (b)

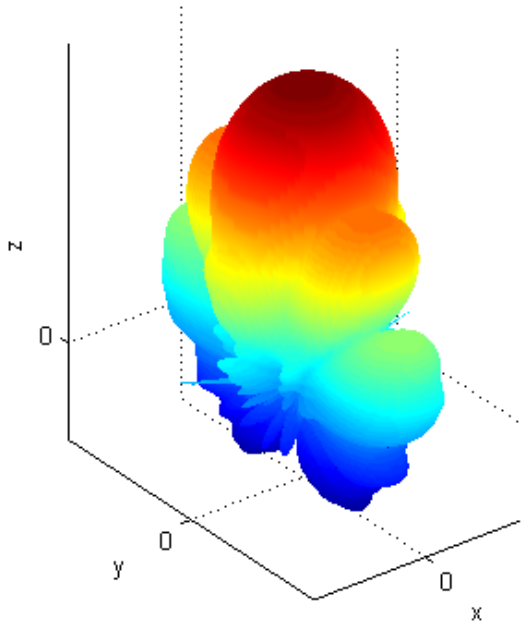

(c)

Figure 4.5: Radiation pattern of the horn antenna: a) Plane E, b) Plane H, c)3-D. Beamwidth $\sim 20\,^{\circ}$

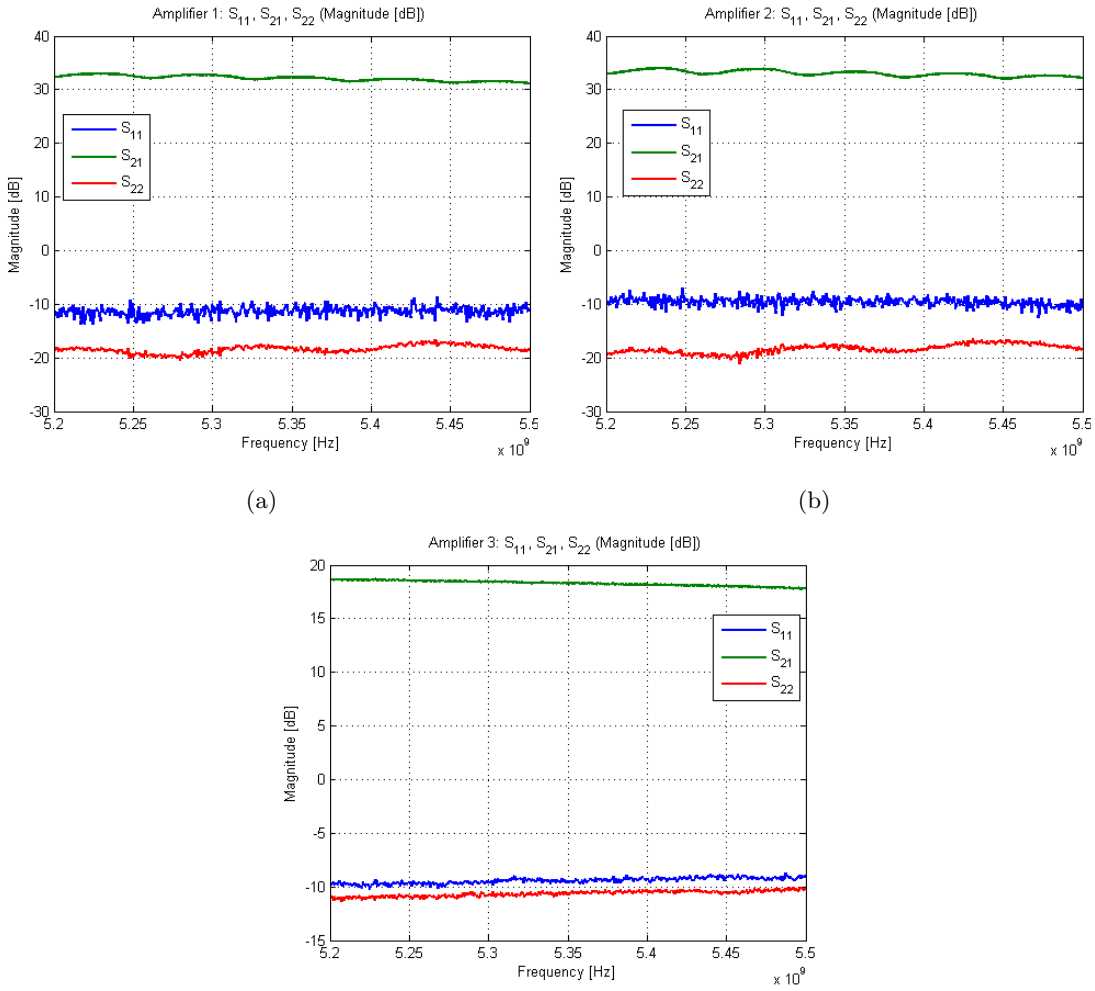

Figure 4.6: $|S_{11}|$, $|S_{22}|$, and $|S_{21}|$ of the three amplifiers used in the PARCs. a) Amplifier-1, b) Amplifier-2, and c) Amplifier-3.

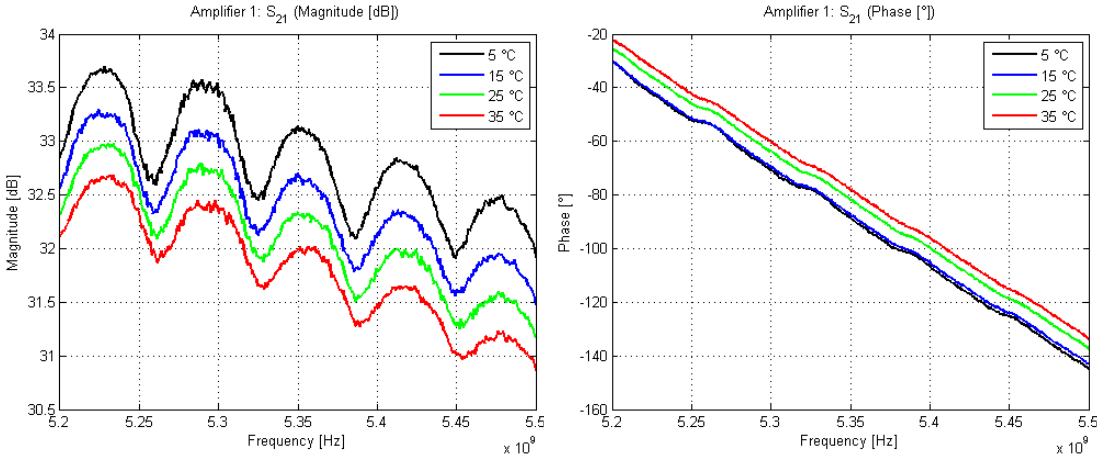

(a) (b)

Figure 4.7: S_{21} of Amplifier-1 at different external temperatures, a) magnitude, b)phase.

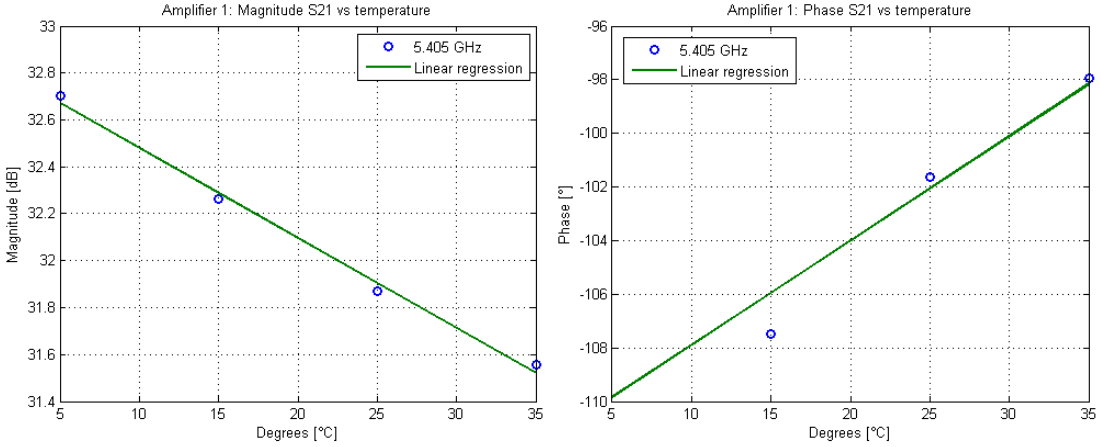

(a) (b)

Figure 4.8: Amplifier 1. a)Magnitude and b)phase of S_{21} as a function of the temperature at 5.4 GHz.

4.3 Outdoor experiments

The desired procedure to perform the measurements is to deploy the three PARCs in different locations in order to use them to calibrate the image. One of the PARC has to be aligned accordingly to the One-PARC configuration, and the others as the Two-PARC configuration. In this way, we can calibrate the image by considering the former configuration, and then the other two PARCs would be control targets. Another option is to perform the calibration by means of the Two-PARC configuration, using the PARC left as a control target. The area selected for the measurements was UPC's Campus North. There, there is proper facilities for deploying the PARC with direct line-of-sight and relatively far (~ 550)m from the SAR detector.

Theoretically, if the PARC's antennas are correctly placed, we should observe the PARCs as bright points on the image of their respective receiving and transmitting polarization. Thus, PARC-1 should be present in all HH, HV, VH and VV images since it S-matrix is full of ones (table 3.1). PARC-2 should be present only in HH and VH images since its receiving antenna is in horizontal polarization. Similarly, PARC-3 should only be present in HV and VV image. In practice, we may found results that are close to the theoretical form of the scattering matrices of the PARCs. The main problem is that the calibration procedure is sensible to errors in the alignment of the antennas, and we also may have errors in the positioning of the control target, for instance, we could have errors of ~ 11 % in the estimation of the S-parameters of a target when we have small angular errors ($\pm 3\,^{\circ}$) in the positioning of the antenna (chapter 3).

In total, there were performed three experiments but in this work it will be presented measurements of the last campaing. We found many problems related with the deployment of the SAR detector in the first campaign. The weight of the horn antennas and the mechanical stability of their support in field conditions were an obstacle for recording data. In the second campaign, two PARCs were too close from each other, overlapping its spots. Finally, in the last campaign, the PARCs were properly placed, but the transmission antennas was found tilted away from it position because its support was loosened from the tripod. Nevertheless, PARC-2 and PARC-3 worked correctly, and the Two-PARC calibration can still be performed but PARC-1 cannot be used as control target.

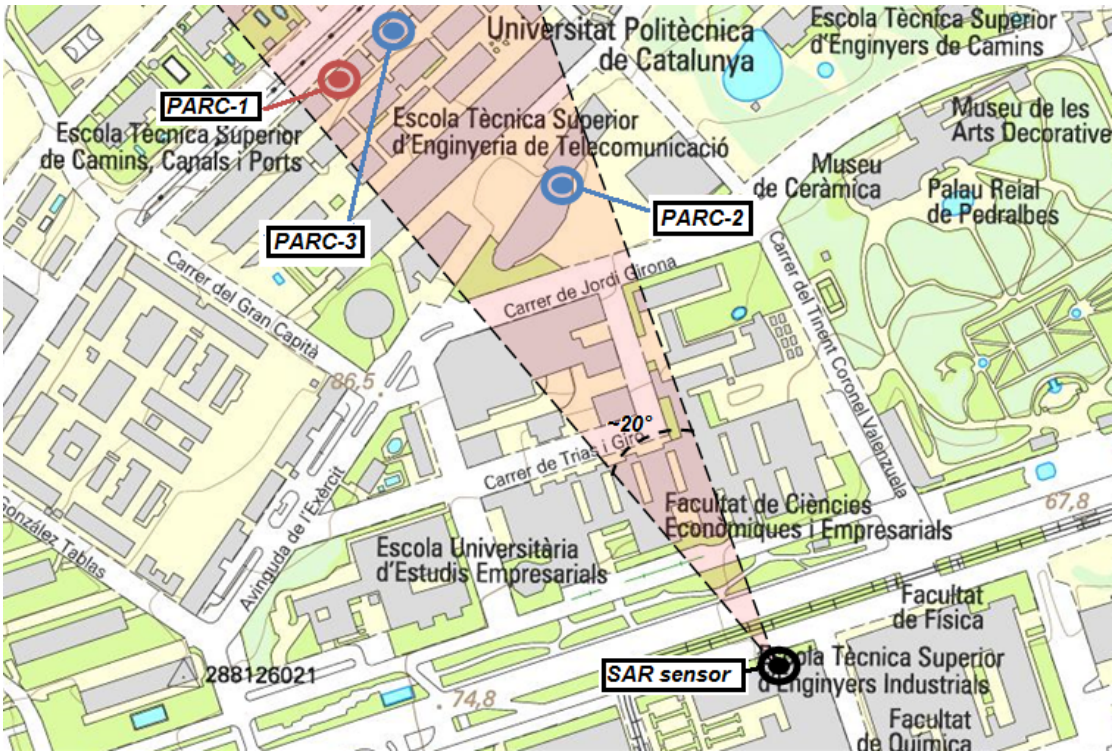

Figure 4.9: Location of the three PARCs and SAR detector. Red dot denotes the ONE-PARC configuration, and Blue dots denote the Two-PARC configuration. The shadowed area represents the 20 ° beamwidth of the SAR sensor's antenna.

4.3.1 Measurements and Results

The following measurements were taken on July 7th 2010. Two PARCs were placed on the roof of the buildings, while the other PARC was placed at ground level on a square. The SABRINA was located on the roof of an opposite building. Figure 4.9 shows the location of each device.

Figure 4.10 shows the images HH, HV, VH, and VV obtained directly of the measurements after the processing of the signal. In order to identify the PARC in the scenes, the images were manually adjusted with a different power scales due to unbalances in the channels. By comparing the images, we can distinguish PARC-3 whose receiving antenna is in V polarization. It presents high power in HV and VV images, while it practically disappears in VH and HH. PARC-2 can be identified by comparing images VH and VV. In the former, we can see it as a high power point, and in the latter it presents a much lower transmission. The locations match with the results of the geocod-

ing application developed for SABRINA. Moreover, this application also suggest that PARC-1 is the spot that appears next to the location of PARC-3 in images VH,HV,and VV.

4.3.2 Calibration

Once we have identified the location of the PARCs, we can calibrate the image by using its respective scattering parameters. In the following, we will use the Two-PARC configuration for the calibration of the image. Moreover, we will assume that the distance from the satellite to each PARC is the same, but the distances to the SAR sensor are 470m, and 602m for PARC-2 and PARC-3, respectively. In this way, each PARC will have the parameter A defined in 3.17 inversely proportional to the distance to the detector.

For the calibration in magnitude, we use the expression 3.5 considering the gain of the antennas $G = 16$dB, effective signal amplification of $G_{A,2} = 18$dB for PARC-2 and $G_{A,3} = 32$dB for PARC-3, and $\lambda = 0.055$m. Afterwards, we measured the peak value of the power over the spot of the corresponding PARC on each image. Then, we apply 3.17 to obtain the four calibrated images as shown in figure 4.11.

In the Two-PARC configuration, the PARC-2 calibrates the images HH and VH, while PARC-3 calibrates images VH and VV. Consequently, we may still have unbalanced images that were calibrated with different PARCs if we do not estimate correctly the gain of each PARC and their distance to the detector.

4.4 Conclusions

The experimental campaign had the objective of evaluating the feasibility of implementing PARCs as control targets for calibration. We found logistic and technical challenges. From one part, there should be enough people in the campaign in order to split efforts between deploying the SAR detector and the PARCs in its locations. Moreover, the experiment requires the deployment, at least, of three PARCs to have the One-PARC configuration and the Two-PARC configuration. From the other part, mechanical junctions are recommended to be tested to detect any loose part that may change the correct alignment of the PARCs' antennas during the campaing. Similarly, it is recommended to test all the electronic devices (batteries, amplifiers, sensors, etc) before the campaign. The temperature has influence in the frequency response of the amplifier in the PARC.

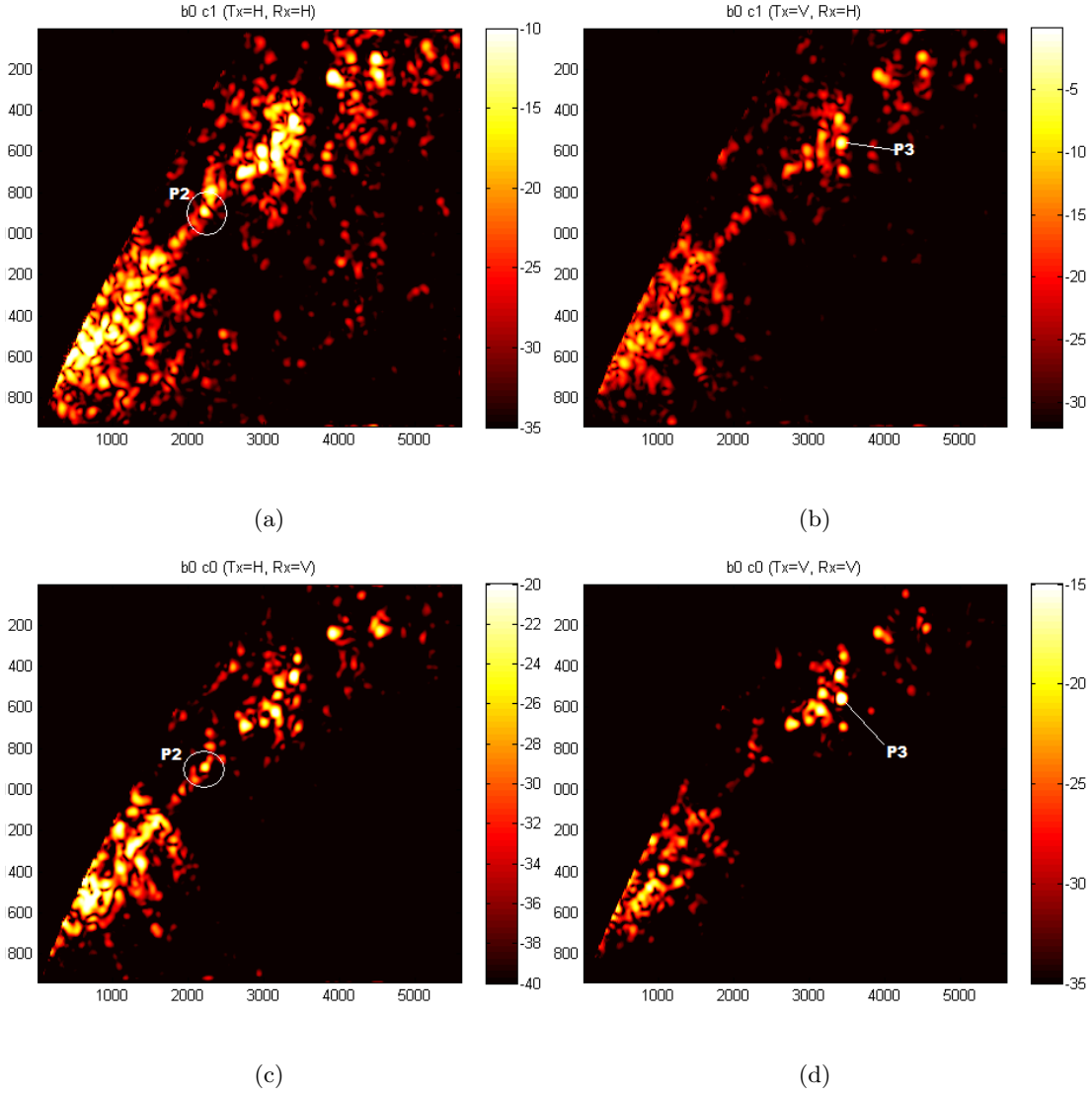

(a) (b)

(c) (d)

Figure 4.10: Direct measurements in dB: a)HH , b)HV, c)VH, d)VV

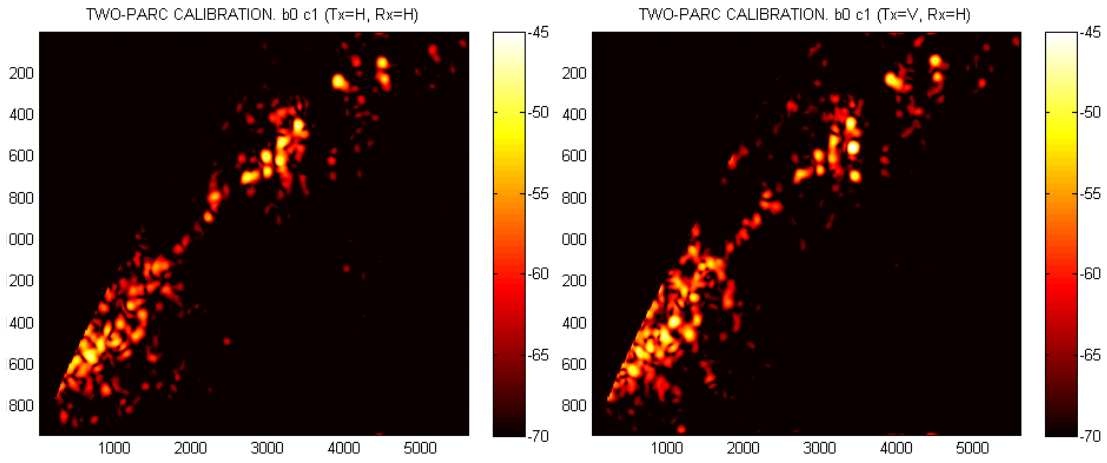

(a) (b)

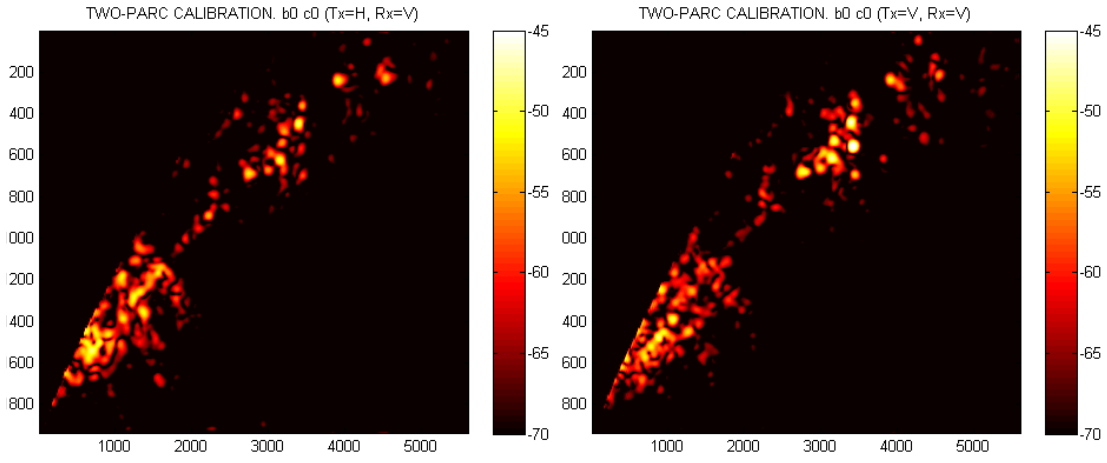

(c) (d)

Figure 4.11: Calibrated measurements in dB with the Two-PARC configuration: a)HH , b)HV, c)VH, d)VV

Hence, for a proper calibration in field conditions, the consideration of the amplifier responses as function of temperature may approach to better results in the calibration. Since the data acquisition window is less than 2 seconds, one could assume that the frequency response is constant during this period of time. Therefore, only one measurement of the temperature at the time of this window would be enough to estimate the frequency response amplifier. The rough approximation made about the distance of the PARCs with respect to the detector and their characteristics (e.g. the effective gain, antennas' gain) provide calibrated images that are qualitatively balanced. Unfortunately, we cannot infer more on how good was the calibration (in relative terms) because of the technical problems with the control target (PARC-1).

Conclusions

The existence of available signals of opportunity in V and H polarizations have motivated the acquisition of polarimetric measurements by using bistatic SAR systems such as SABRINA. For the proper interpretation of the data, the measurements require calibration. In this work, we have studied a polarimetric calibration procedure based on active devices that can be applied to SABRINA-like systems.

The direct polarimetric measurements represent a distorted version of the correct scattering matrices of the targets. Through the calibration, we suppressed error related to the frequency response of the electronic devices, channel imbalance and mismatches in the hardware. In our system, we took advantage of the high polarization isolation to simplify the calibration procedure. Moreover, that also relaxed the amount of independent control target to solve the system and obtain the calibration parameters. As a consequence, a minimum of one control target is required.

We considered two cases for the calibration: the One-PARC configuration and the Two-PARC configuration. We found that the former may induce more errors in the estimation of the calibration coefficients because of its higher sensitivity to errors in the alignment of receiver antenna. However, such error would be reflected as an offset in all channels. On the contrary, the Two-PARC configuration presented much less sensitivity to errors in the alignment of the receiver antenna, but we can have different offsets between two channels since each PARC calibrates two of the four channels. In this configuration, perfect characterization of the PARCs is required in order to have balanced channels.

Finally, the feasibility of the calibration using either the One-PARC or Two-PARC configuration has been proved. However, the logistic of campaign and the prototype structure of the PARCs must be refined to foreseen possible problem during the measurements. From the experiences of the campaigns, the recommendations are:

- A team of five or six people in the campaign in order to split efforts in the deployment of the PARCs and SAR detector.
- Verification of the mechanical and electrical part of the PARCs before each campaign.
- In the One-PARC configuration the antenna has to point to the satellite with the proper rotation. For an easier deployment in field, it would be desirable to have a structure with the receiving antenna already rotated and fixed, providing only degree of freedom in azimuth and altitude.
- Deployment of spare control points
- Pictures of the scenes around the detector and the PARCs. Pictures from the line-of-sight of the antennas may provide information to identify targets from the scattered radiation.

The following lines of work are identified in order to enhance the calibration:

- Full characterization of the scattering behavior and frequency response of the PARCs by taking into account the chain from the receiving antenna to the transmitting antenna.
- Experimental validation of the calibration procedure with the full characterized PARCs.
- Extension of the calibration procedure considering that the cross-talk between channels is low but not zero.

Appendix A

Experimental Measurements

A.1 Frequency response of amplifiers 2 and 3

Measurements of the frequency response (C-band) of the amplifiers 2 (figure A.1) and 3(figure A.2) for different temperatures: climatic chamber from 5 °C to 35 °C with a 10 °C step.

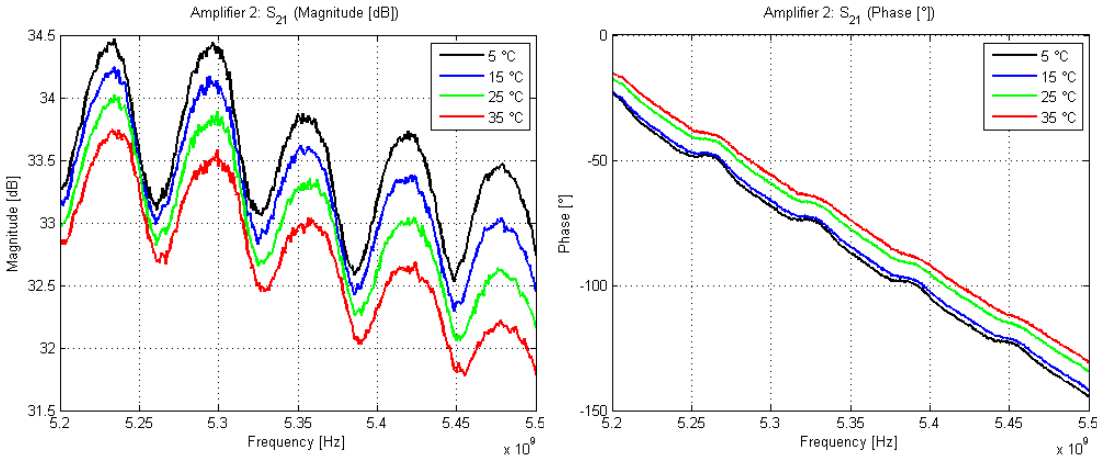

(a) (b)

Figure A.1: S_{21} of Amplifier-2 at different external temperatures, a) magnitude, b)phase.

For RADARSAT-2's operating frequency, figure A.3 and A.3 show the magnitude and phase of S_{21} as a function of the temperature for amplifier 2 and 3, respectively.

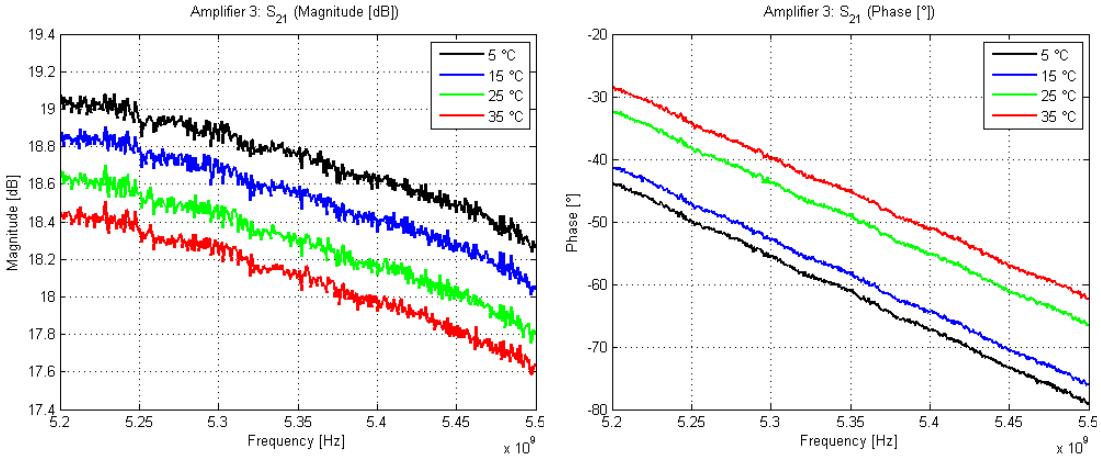

(a) (b)

Figure A.2: S_{21} of Amplifier-2 at different external temperatures, a) magnitude, b)phase.

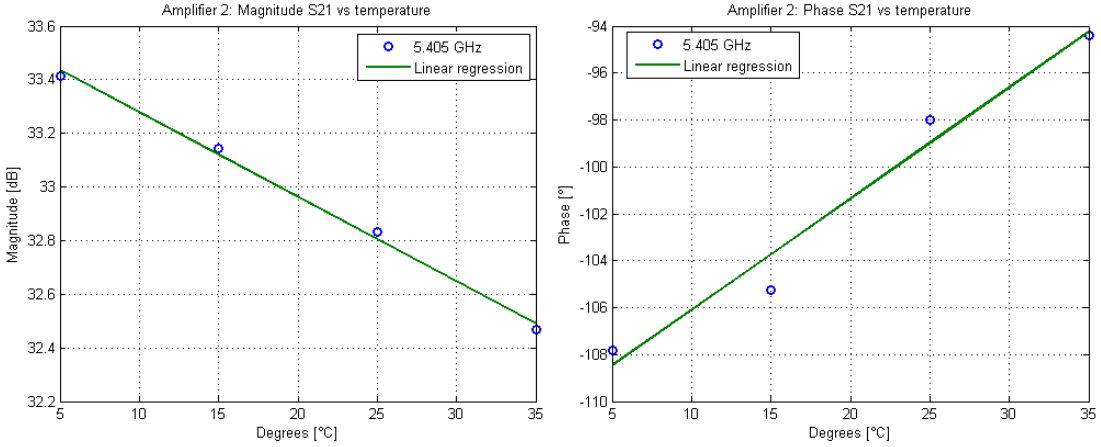

(a) (b)

Figure A.3: Amplifier 2. a)Magnitude and b)phase of S_{21} as a function of the temperature at 5.4 GHz.

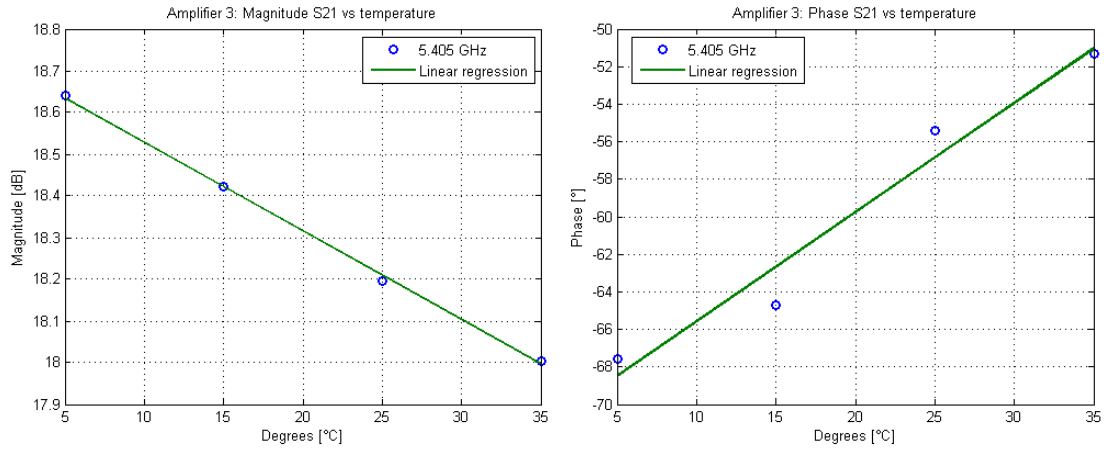

(a) (b)

Figure A.4: Amplifier 3. a)Magnitude and b)phase of S_{21} as a function of the temperature at 5.4 GHz.

References

[1] J. A. Richards, *Remote Sensing with Imaging Radar*. Springer, 2009.

[2] H. Zebker and J. Van Zyl, "Imaging radar polarimetry: a review," *Proceedings of the IEEE*, vol. 79, pp. 1583 –1606, nov 1991.

[3] A. Freeman, "Sar calibration: an overview," *Geoscience and Remote Sensing, IEEE Transactions on*, vol. 30, pp. 1107 –1121, nov 1992.

[4] D. Kahny, K. Schmitt, and W. Wiesbeck, "Calibration of bistatic polarimetric radar systems," *Geoscience and Remote Sensing, IEEE Transactions on*, vol. 30, pp. 847 –852, sep 1992.

[5] C. Bradley, P. Collins, J. Fortuny-Guasch, M. Hastriter, G. Nesti, J. Terzuoli, A.J., and K. Wilson, "An investigation of bistatic calibration techniques," *Geoscience and Remote Sensing, IEEE Transactions on*, vol. 43, pp. 2185 – 2191, oct. 2005.

[6] J. Sanz-Marcos, P. Lopez-Dekker, J. Mallorqui, A. Aguasca, and P. Prats, "Sabrina: A sar bistatic receiver for interferometric applications," *Geoscience and Remote Sensing Letters, IEEE*, vol. 4, pp. 307 –311, april 2007.

[7] R. J. Sullivan, *Radar Foundations for Imaging and Advanced Concepts*. SciTech Publishing Inc., 2004.

[8] C. A. Balanis, *Antenna Theory. Analysis and Design*. Wiley, third ed., 2008.

[9] S. Cloude, *Polarisation: aplications in remote sensing*. Oxford University Press, 2010.

[10] I. Sikaneta, C. Gierull, S. Chiu, and P. Beaulne, "Radarsat-2 System and Mode Description," *Integration of Space-Based Assets within Full Spectrum Operations, Meeting Proceedings RTO-MP-SCI-150*, vol. 4, Issue:2,, pp. 15–1 15–22, 2005.

[11] W. Wiesbeck and S. Riegger, "A complete error model for free space polarimetric measurements," *Antennas and Propagation, IEEE Transactions on*, vol. 39, pp. 1105 –1111, aug 1991.

[12] A. Freeman, Y. Shen, and C. Werner, "Polarimetric sar calibration experiment using active radar calibrators," *Geoscience and Remote Sensing, IEEE Transactions on*, vol. 28, pp. 224 –240, mar 1990.

[13] J. Extremadura, *Diseño, construcción y caracterización de un calibrador activo para dispersómetro polarimétrico.* Projecte Final de Carrera, Universitat Politècnica de Catalunya (UPC), 1997.

[14] D. R. Brunfeldt and F. T. Ulaby, "Active reflector for radar calibration," *Geoscience and Remote Sensing, IEEE Transactions on*, vol. GE-22, pp. 165 –169, march 1984.

[15] J. Sanz-Marcos, J. Mallorqui, A. Aguasca, and P. Prats, "First envisat and ers-2 parasitic bistatic fixed receiver sar images processed with the subaperture range-doppler algorithm," in *Geoscience and Remote Sensing Symposium, 2006. IGARSS 2006. IEEE International Conference on*, july 2006.